Applied Catalysis B: Environmental 237 (2018) 491–503

Contents lists available at ScienceDirect

Applied Catalysis B: Environmental

journal homepage: www.elsevier.com/locate/apcatb

Photo-assisted methanol oxidation on Pt-TiO_2 catalysts for direct methanol fuel cells: A short review

Ermete Antolini

Scuola di Scienza dei Materiali, Via 25 aprile 22, 16016 Cogoleto, Genova, Italy

ARTICLE INFO

Keywords:
Direct methanol fuel cell
Methanol oxidation
Platinum
Titanium oxide
Photocatalysis

ABSTRACT

Platinum and platinum-based electrocatalysts for the methanol oxidation reaction (MOR) are commonly used as the anode material in direct methanol fuel cells (DMFCs). Photo-oxidation promoted by ultraviolet and visible light is a promising method to increase the catalytic activity of DMFC anode electrocatalysts. Photocatalytic and electrocatalytic methanol oxidation can be coupled by addition of TiO_2, a semiconductor photocatalyst, to Pt. In the presence of TiO_2, an increase of the MOR activity of Pt-based electrocatalysts takes place also in dark conditions. This review deals with the methanol photo-oxidation on Pt/TiO_2 catalysts, highlighting the effect of TiO_2 morphology, nanoparticles, or 1D nanostructures, on the MOR activity under illumination. Comparison of reaction mechanisms in the presence and the absence of light are presented, and the roles of Pt and TiO_2 during electrochemical and photochemical reactions are discussed.

1. Introduction

Direct methanol fuel cells (DMFCs) represent an efficient tool to transform chemical energy to electrical energy [1]. Carbon supported platinum is commonly used as the anode catalyst in low-temperature fuel cells. The activity for the methanol oxidation reaction (MOR) of Pt alone, however, is too low for an industrial use, thus research efforts have been addressed to improve the MOR activity of platinum. A way to increase the catalytic activity is the addition of a second metal, in particular ruthenium, to Pt [2]. According to the bifunctional mechanism, the second metal supplies oxygen to oxidise the Pt-adsorbed methanol oxidation intermediate species, while according to the electronic effect, the second metal modifies the Pt electronic configuration, weakening the adsorption of methanol oxidation intermediate species on Pt [3]. Photo-assistance is another way to improve the methanol oxidation on Pt-based catalysts. The MOR activity of Pt can be improved under UV–vis (UV–vis) light irradiation by addition of TiO_2 [4], a semiconductor photocatalyst, coupling photocatalytic and electrocatalytic mechanisms of methanol oxidation, and giving rise to a novel type of DMFCs, namely photo-assisted direct methanol fuel cells (PDMFCs), as shown in Scheme 1 [5]. In this way, the fuel cell performance can be improved by conversion of chemical energy and solar light energy to electrical energy. Before its new role as a photocatalysis promoter in Pt-based catalysts, TiO_2 has been proposed as a support (alone or carbon-mixed) and/or as an additive to improve the MOR activity of Pt and Pt-based catalysts for DMFCs operating in dark conditions [6–8]. In this work an overview of the photo-assisted methanol oxidation on Pt/TiO_2 and PtM/TiO_2 (M = Ru, Ni) catalysts is presented. The synergic effect of Pt and TiO_2 in enhancing the activity for methanol oxidation and the tolerance to methanol oxidation intermediate species poisoning in the presence of light is discussed. To better understand the photo-assisted methanol oxidation on Pt/TiO_2 catalysts, short parts regarding the methanol oxidation on Pt-TiO_2 catalysts in dark conditions and the photo-assisted methanol oxidation on Pt and TiO_2 alone are also reported. A brief section on other semiconductors than TiO_2, which may also cooperate with Pt to enhance the MOR activity under light illumination is also included in this work.

2. Effect of TiO_2 as a support and/or an additive material on the activity for methanol oxidation of platinum in dark conditions

The activity of a catalysts can be expressed as the specific activity (SA) and the mass activity (MA). In electrochemistry the SA is an intrinsic characteristics of a material and is expressed as the current density at a given potential (i_V) to the real Pt surface area (A_r), generally measured by cyclic voltammetry (CV), ratio ($SA = i_V/A_r$) [9]. The MA is expressed as the ratio between the roughness factor (r_f) and the Pt loading on the catalyst surface, (L_P,) ($MA = r_f/L_P$), where r_f is the ratio between the real Pt surface area and the geometric area of the electrode. MA is an important parameter as the cost of the fuel cell depends in a large extent on the amount of precious metal in the catalyst. The relation between SA and Ma is:

$$MA = SA * ECSA \quad (1)$$

E-mail address: ermantol@libero.it.

https://doi.org/10.1016/j.apcatb.2018.06.029
Received 10 April 2018; Received in revised form 8 June 2018; Accepted 9 June 2018
Available online 10 June 2018
0926-3373/

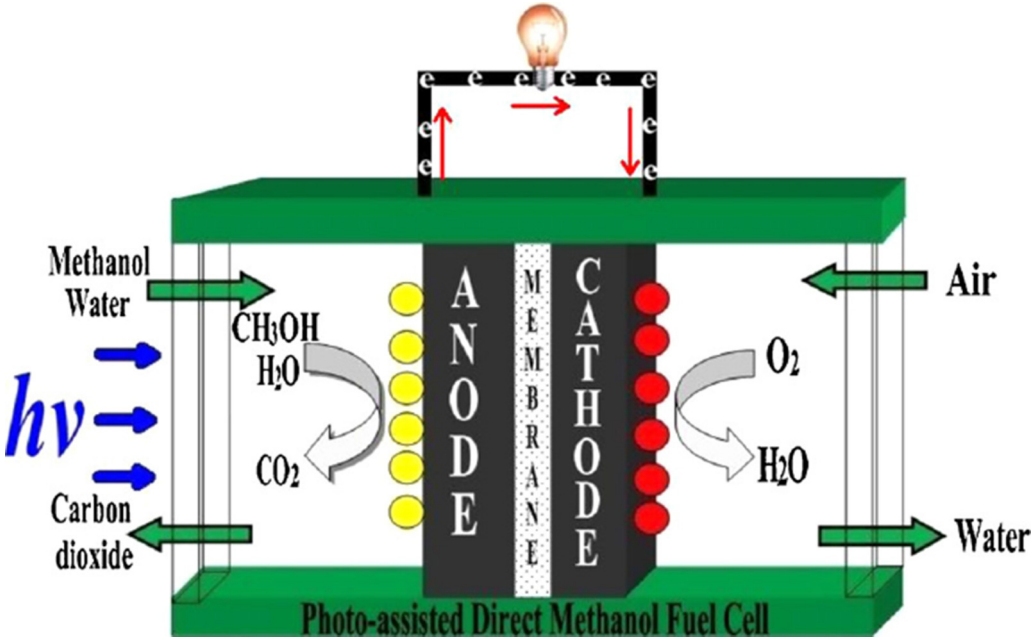

Scheme 1. Schematic operation principle of photo-assisted direct methanol fuel cell. Reproduced from Ref. [5], copyright 2013, with permission from Elsevier.

where the ECSA is the electrochemical surface area per Pt content, calculated by CV or by CO stripping measurements. The catalytic activity of supported catalysts is lowered by the electrochemical corrosion of the carbon substrates, which gives rise to the migration and aggregation of platinum nanoparticles [10]. Ceramic oxides, such as TiO_2, SnO_2 and WO_3, have been proposed as corrosion-resistant catalyst supports [6]. Moreover, unlike carbon, many metal oxide can act as co-catalysts, reducing Pt poisoning by removing adsorbed methanol oxidation intermediate species on the catalyst surface [6]. Among different inorganic metal oxides, due to its catalytic properties and its excellent resistance to corrosion in various electrolytic media [11,12], titanium dioxide is widely used as support/co-catalyst in fuel cell anode materials. The drawback to the use of TiO_2 as catalyst support, however, is its poor electrical conductivity and low surface area, giving rise to a low Pt nanoparticle dispersion. To overcome this hindrance, the use of TiO_2 mixed with or supported on carbon materials (increased conductivity and area), such as carbon black (C), carbon nanotubes (CNTs) and graphene (GNs), and/or in a nanostructured form (high surface area), such as titanium oxide nanotubes (TONTs) and nanowires (TONWs), was suggested. The structural and electrochemical characteristics of some Pt-TiO_2 catalysts are shown in Table 1 [13–30]. As can be seen in Table 1, in the most part of catalysts TiO_2 is present together with a carbon material or in a nanostructured form. The Pt/TiO_2 to Pt MOR specific activity ratio ($SA_{P/TiO2}/SA_{Pt}$) of all the catalysts was > 1, indicating a positive effect of TiO_2 presence on the activity for methanol oxidation of Pt. The Pt/TiO_2 to Pt MOR mass activity ratio ($MA_{P/TiO2}$-MA_{Pt}) of the most part Pt/TiO_2 catalysts (76%) was > 1, while the remaining part of Pt/TiO_2 catalysts (24%) showed a $MA_{P/TiO2}MA_{Pt}$ ratio < 1. The $MA_{P/TiO2}MA_{Pt}$ ratio < 1 was observed overall for Pt supported on low surface area TiO_2 nanoparticles (TONPs) in the absence of carbon. The comparison of MOR onset potential of Pt/TiO_2 and Pt confirm the results of SA and MA: the most part of TiO_2-containing catalysts presented a MOR onset potential lower or even than that of Pt alone (73%). The remaining part of Pt/ Pt/TiO_2 catalysts (27%) showed a MOR onset potential higher the that of Pt. As in almost all the cases these catalysts presented also a $MA_{P/TiO2}MA_{Pt}$ ratio < 1, the higher onset potential has to be ascribed to the large Pt particle size, due to the low surface area of TiO_2 particle. Moreover, the presence of TiO_2 results in a higher ratio of the anodic peak current density in the forward scan (I_f) to that in the reverse scan (I_b), (I_f/I_b) by cyclic voltammetry (CV)

Table 1
Difference between the MOR onset potential of Pt/TiO_2 and that of Pt ($\Delta V_o(PtTiO_2,Pt)$), Pt/TiO_2 to Pt MOR specific activity ratio (SA_{PtTiO2}/SA_{Pt}), and Pt/TiO_2 to Pt MOR mass activity ratio (MA_{PtTiO2}/MA_{Pt}) in dark conditions. (+) $\Delta V_o(PtTiO_2,Pt) > 0$; (-) $\Delta V_o(PtTiO_2,Pt) < 0$; (=) $\Delta V_o(PtTiO_2,Pt) = 0$.

Catalyst	$\Delta V_o(PtTiO_2,Pt)$	SA_{PtTiO2}/SA_{Pt}	MA_{PtTiO2}/MA_{Pt}	Reference
Pt/C/TiO_2nanorods	+	1.69	0.63.	[13]
Pt/C/TONT	–	1.31	1.73	
$(PtRu)_{50}(TiO_2)_{50}$	–	3		[14]
Pt/GN/TONP(40%)	–	1.33	1.46	[15]
Pt/TONT	=	> 1	> 1	[16]
Pt/TONP	=	> 1	> 1	
Pt/C-TiO_2	=		1.57	[17]
Pt/C-TONT	=	> 1	> 1	[18]
Pt/Gs/TiO_2	=	1.27		[19]
Pt/porousTiO_2	–			[20]
Pt-TiO_2/CNT	–	1.44		[21]
PtRu/TiO_2/C	=	> 1	> 1	[22]
Pt/TiO_2anatase	–		2.16	[23]
Pt/TiO_2(two phases)	–		2.56	
Pt/TiO_2-C	–		1.86	[24]
Pt/TiO_2-C 10%	–	1.38	2.49	[25]
30%	–	2.56	2.35	
60%	–	1.69	2.16	
Pt/C-OMTiO_2	=		1.5	[26]
Pt/TiO_2	+		0.5	
Pt/TiO_2	+	4.5	0.85	[27]
Pt/C-TiO_2	+	3	0.61	
PtRu/TiO_2/CNF	–		4	[28]
PtRu/C-TiO_2	+		1.30	
PtRu/TiO_2	+		0.072	
Pt/TiO_2/PDA	–	1.8		[29]
Pt/CNT/TiO_2	+	> 1	< 1	[30]

[13,16,20,23,24,26,30], reflecting a higher poisoning tolerance, a higher short time stability by chronoamperometry (CA) [17,19,24,29,30], also related to the poisoning tolerance, and a higher long time durability by repetitive potential cycling (RPC) [13,15,18,24,26], indicative of the structural stability, that is, a lower support corrosion and a lower electrochemically active surface area (ECSA) decrease than Pt alone.

Electrochemical impedance spectroscopy (EIS) measurements were

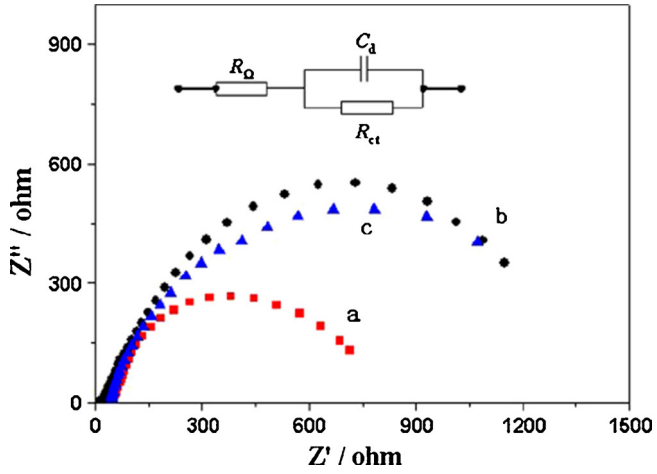

Fig. 1. Nyquist plots of EIS for MOR in the N_2 saturated solution of 1M CH_3OH + 0.5M H_2SO_4 at 0.5V in the frequency range of 100 kHz to 0.1 Hz: Pt/TiO_2/GNs (a), Pt/GNs (b) and Pt/C-JM (c). Reproduced from Ref. [31], copyright 2014, with permission from Elsevier.

used to further investigate the effect of TiO_2 presence on the MOR activity of Pt, by evaluating the charge transfer kinetics of methanol oxidation [18,29,31,32]. Generally, it was found that in the presence of TiO_2 the electron transfer rate of methanol oxidation accelerated. For example, the Nyquist plots of EIS for Pt/TiO_2/GNs, Pt/GNs and Pt/C-JM in a CH_3OH/H_2SO_4 solution at 0.5 V are shown in Fig. 1 [31]. The diameter of the semicircle in low frequency region is associated with the charge transfer resistance (R_{ct}) of the catalyst, related to the rate of charge transfer during the methanol oxidation. The semicircle diameter of Pt/TiO_2/GNs is smaller than those of Pt/GNs and a commercial Pt/C, indicating that TiO_2 presence enhances the conductivity of Pt. Although TiO_2 is a semiconductor, its presence up to a certain value can increase the conductivity of the catalyst. The interaction between platinum active sites and the metal oxide could enhance the charge transfer at the interface. But an excessive amount of TiO_2 could block some platinum active sites, thus decreasing the electrical conductivity of the catalyst. Finally, EIS measurements carried out on Pt/C-TONTs and Pt/C-TONPs showed that the R_{ct} of Pt/C-TONTs catalyst is lower than that of Pt/C-TONPs [18], indicating that the electronic conductivity of TONTs is higher than that of TONPs.

The enhanced MOR activity of Pt in the presence of TiO_2 can be ascribed to both the bifunctional mechanism and the electronic effect [33]. On one hand, TiO_2 can easily adsorb −OH species, which can oxidise Pt-adsorbed methanol oxidation intermediate poisoning species, leaving the active site available for subsequent electrochemical reactions. Theoretical studies showed that spontaneous dissociative H_2O adsorption effectively occurs on the (001) TiO_2 surface, whereas molecular H_2O adsorption is prevalent on the (101) surface [34]. The commonly used P25 titanium oxide contains more than 70% anatase. Because the crystallite shape of anatase is a truncated bipyramid exposing both the (101) and (001) surfaces, a large quantity of (001) surface planes can be supply by TiO_2. So, dissociative H_2O adsorption on the (0 01) anatase surface will form plentiful Ti−OH surface groups, furthering CO electro-oxidation on the Pt catalyst by the bifunctional mechanism. On the other hand, the electronic interaction between Pt and TiO_2 modifies the electronic properties of Pt by changing the electron density of the states of the d-band and Fermi level energy. Indeed, by XPS measurements a positive shift of the Pt 4f binding energies for Pt/C/TiO_2 relative to the Pt/C values was observed, suggesting an interaction between Pt and TiO_2, which changes the electronic and catalytic properties of Pt nanoparticles [13]. The electronic structure of Pt atoms can considerably modified by the hypo–hyper-d-electron interaction between TiO_2 and Pt particles. So, the CO oxidation activity on Pt surface can be enhanced if the change of the adsorption strength of CO adsorbed species can therefore decrease the activation barrier for the CO oxidation reaction. Moreover, the diffusivity of adsorbed species on Pt particles, strongly interacting with TiO_2, may be significantly modified. The CO surface diffusivity on the Pt nanoparticle can be enhanced by the weakened CO adsorption strength on Pt nanoparticles [35]. Due to the small size (commonly < 5 nm) of Pt catalyst particles, CO and/or OH adsorbed species can readily diffuse over the Pt nanoparticle, supporting a better efficiency of CO oxidation by the Langmuir–Hinshelwood reaction mechanism, which supposes that adsorbed reactants diffuse, collide and form products on the surface.

Moreover, a high Pt utilization, due to the enhanced metal dispersion and the formation of smaller metal particles, and a good electron conductivity can be obtained up to a certain amount of TiO_2 nanoparticles. The effect of TiO_2 loading on the SA and MA goes through a maximum, which is higher for the SA than MA (60 *vs.* 40% TiO_2 [15], and 30 *vs.* 10 TiO_2 [25]: indeed, the ECSA decreases with increasing TiO_2 content, because TiO_2 particles cover the Pt nanoparticle surface and hinder methanol to reach the active sites. In a rough approximation, at a fixed particle size, the SA and ECSA of Pt/TiO_2 catalysts depend on TiO_2 content (x_T) as:

$$SA = SA_o + k\,x_T - k'(x_T)^2 \quad (2)$$

$$ECSA = ECSA_o - k''x_T \quad (3)$$

where SA_o and $ECSA_o$ are the values of SA and ECSA for $x_T = 0$, and k, k' and k''(all > 0) are constants depending on different parameters such as particle size, crystal structure and surface segregation. The parabolic dependence of SA on the fraction of TiO_2 is due to the initial increase of the catalytic activity of Pt in the presence of TiO_2, as previously reported, and the decrease of the MOR activity for high TiO_2 contents, owing to the concomitant decrease of the fraction of Pt active sites. From Eq. (2), it can deduce that SA goes through a maximum, and from Eqs. (1)–(3), it results that the x_T maximum for MA is lower than x_T maximum for SA.

Finally, the strong metal-support interaction between Pt and TiO_2 can anchor the Pt nanoparticles, improving the structural stability of the catalysts in a considerable way.

3. Photo-assisted methanol oxidation

3.1. Photo-assisted MOR on TiO2

Titanium oxide is one of the most used photocatalysts for its efficiency, low cost, high stability and non-toxicity. TiO_2 can form three crystalline phases two of which, anatase and rutile, are photocatalytically active. A problem associated with the use of TiO_2 is related to its large band gap (3.0 eV in the rutile and 3.2 eV in the anatase phase), as a result of which titania can only absorb ultraviolet (UV) light. To a full use of the solar energy and to increase the photocatalytic efficiency, the band gap of TiO_2 has to be reduced into the range in which visible (Vis) light can be absorbed. The main ways to overcome this drawback are i) doping TiO_2 by an appropriate amount of metal ions, such as Fe^{3+}, Cr^{3+}, Ru^{2+}, Ce^{4+}, La^{3+} and V^{5+}, or by nonmetals, such as N, C, F, B, and ii) forming a hybrid nanostructure comprising TiO_2 and a noble metal such as Pt, Au or Ag [36–38]. Considering the topic of this review, the last case is the most interesting. The optical properties of TiO_2 (100% anatase) and M/TiO_2 (M = Pt, Pd and Au) samples were evaluated by comparing their UV–vis diffuse reflectance spectra (Fig. 2a) [39]. UV–vis spectra were also recalculated in the Kubelka-Munk coordinates (Fig. 2b). The spectrum of TiO_2 showed a broad absorption region below 400 nm, ascribed to the charge transfer from the valence band to the conduction band of TiO_2. The M/TiO_2 hybrids showed the same absorbance in UV region. But in visible region, the M/TiO_2 hybrids showed much higher absorbance than TiO_2. Such behavior was ascribed to the light absorbance due to the

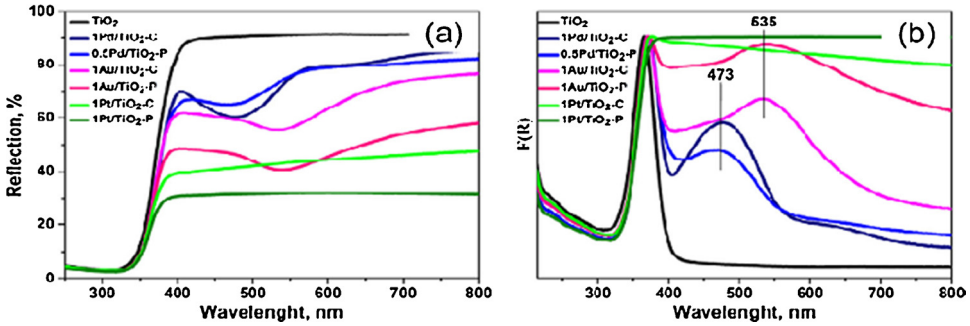

Fig. 2. UV–vis diffuse reflectance spectra (a) and their recalculation in the Kubelka-Munk coordinates (b). Reproduced from Ref. [39], copyright 2017, with permission from Elsevier.

excitation of electrons in metal particles. The increase of the absorbance with increasing metal content confirmed this assumption. However, the cause for the enhanced light absorption of TiO_2 in the presence of Pt at visible region is not clearly established. Au has the typical surface plasmon resonance (SPR) absorption that can sensitize TiO_2 to exhibit photoresponse at visible region. Pt on the contrary does not show SPR effect at visible region and therefore fails to sensitize TiO_2 to visible light. The descriptions regarding the enhanced visible absorption due to the electron transfer from Pt to TiO_2 did not comply with the general sense. The contention of electron transfer from Pt to TiO_2 induced by Schottky barrier [40] was also controversial. Another drawback is that electron/hole pairs ($e-/h+$) formed by TiO_2 irradiation tend to recombine, decreasing the photonic efficiency. TiO_2-NCs (NCs = nanocarbon such as CNTs and GNs) composites are a suitable tool for enhancing the separation of photo-generated electron/hole pairs, due to the high electric conductivity of carbon nanomaterials. It is well known that CNTs synergistically improve the photocatalytic activity of TiO_2 by the retardation of electron/hole recombination [41]. In the presence of CNTs, photogenerated electrons can move towards the CNT surface, which may have a lower Fermi level. In this way CNTs act as an electron sink. The excess of holes in TiO_2 valence band can migrate to the surface and react. For example, Yao et al. [42] compared charge recombination by measuring the photoluminescence spectra of bare TiO_2 and TiO_2-CNT composites. A TiO_2-CNT composite in an optimal composition showed enhanced and selective photocatalytic oxidation of phenol than both pure anatase and anatase/rutile mixed phase. According to the proposed mechanism, electrons are shuttled from TiO_2 particles to the CNTs, thus stabilizing charge separation and reducing charge recombination. Analogously, the formation of heterostructures in M/TiO_2 (M = noble metal) photocatalysts play a key role in the retardation of e^-/h^+ recombination [38]. Photogenerated electrons transfer from the conduction band of TiO_2 to the metal particles, while the photogenerated holes remain/migrate on TiO_2 surface, reducing charge recombination. For most of the Pt/TiO_2 composite photocatalyst systems, electron transfer from TiO_2 to Pt is considered because Pt functions an effective electron acceptor, which has nothing to do with Schottky barrier.

The comparison of the MOR photoactivity of well-defined TiO_2 single-crystal anatase (101) surfaces with that of rutile single crystal (001), (100), and (110) surfaces showed that the anatase (101) surface possess a higher photocatalytic activity than all investigated rutile surfaces [43]. Considering that anatase (101) and rutile (110) are the thermodynamically most stable surfaces, this explain the higher photocatalytic activity for methanol oxidation of anatase nanoparticles than that of the rutile ones. It was observed that mesoporous rutile holes are less effective than mesoporous anatase holes to drive efficient and irreversible methanol oxidation [44]. On anatase the C–H bond is first cleaved by a surface hole forming the $\cdot CH_2OH$ radical. Contrary to anatase, the methanol must first dissociate on the rutile surface to form absorbed methoxy groups before C—H bond cleavage can occur, which is the reason why slower/more reversible scavenging kinetics are observed. A very efficient TiO_2 photocatalyst, however, consists of *ca.* 75% anatase and 25% rutile, known as P25. The effectiveness of this composition is due to the fact that rutile has a conduction band lower than that of anatase and this allows electron transfer from anatase to rutile, decreasing electron-hole recombination probability [45].

The methanol photo-oxidation takes place in the following way: when TiO_2 is irradiated with UV an electron/hole pair ($e-/h+$) is generated by promotion of an electron from the valence band (VB) to the conduction band (CB) [36]:

$$TiO_2 + h\nu \rightarrow h^+ + e^- \quad (4)$$

Then hydroxyl radicals ($OH\cdot$) are formed by the oxidation of H_2O molecules or $OH-$ ions adsorbed on TiO_2 surface, according to:

$$h^+ + H_2O \rightarrow OH\cdot + H^+ \quad (5)$$

$$h^+ + OH^- \rightarrow OH\cdot \quad (5')$$

Finally, methanol can be oxidized by $OH\cdot$ radicals (indirect oxidation) [46] (Eqs. (6) and (7):

$$CH_3OH + OH\cdot \rightarrow CH_2OH\cdot + H_2O \quad (6)$$

$$CH_2OH\cdot \rightarrow HCHO + H^+ + e^- \quad (7)$$

or the holes can oxidizes methoxy species from methanol (direct oxidation) as the following equations [47]:

$$CH_3O^- + h^+ \rightarrow CH_3O\cdot \quad (8)$$

$$CH_3O\cdot \rightarrow HCHO + H^+ + e^- \quad (9)$$

Chen and Henderson [48] found that adsorbed methoxy is at least an order of magnitude more reactive than molecularly adsorbed methanol for hole-mediated photo-oxidation. Methoxy photodecomposes through cleavage of a C—H bond forming adsorbed formaldehyde. These results suggest that methoxy, and not molecular methanol, is the effective hole scavenger in photochemical reactions of methanol on TiO_2. Thus, the primary pathway for initial methanol adsorption on TiO_2 is dissociative, leading to the production of adsorbed methoxy groups. The negative charge of the methoxy species gives rise to band-bending in the near-surface region. The resulting electric field inside the material splits the electron-hole pairs, reducing the recombination probability and facilitating hole migration toward the surface [49,50]. But the main advantage of the methoxy group over methanol is the hole transfer between the substrate and the adsorbed species: while the transfer is energetically favorable for the methoxy, an isolated adsorbed methanol molecule cannot trap holes as the presence of the proton bound to the O, inhibiting the hole transfer [50].

Excluding noble metals, the MOR activity of TiO_2 can be considerably improved by using TiO_2-NCs composites [51–54] and titanium oxide nanotubes (TONTs) [55–66]. TiO_2-NC composites are promising photocatalysts because carbon materials, in addition to

possessing a high surface area and a high electrical conductivity, reduce the band gap of TiO_2 into the range of visible light adsorption, reduce the electron/hole recombination and provide highly adsorptive active sites [41]. The improvement of the photocatalytic activity of TiO_2-NC composites for methanol oxidation is mainly due to the increased charge carrier separation rate at the TiO_2 and carbon interface. Dechakiatkrai et al. [51] compared the photocatalytic activity for methanol oxidation of TiO_2-CNTs in acid environment under UV illumination. The presence of carbon nanotubes in the TiO_2 film resulted in a MOR activity 10 times higher than bare TiO_2. Sellapan et al. [52]

investigated the methanol photo-oxidation on TiO_2-GN composites using graphene prepared by different methods. All graphene-containing composites showed considerably higher photocatalytic MOR activity than bare TiO_2 films. The activity of the composites depended on the electrical conductivity and surface roughness of the respective carbon structure. In the same way, the photocatalytic activity for methanol oxidation of a TiO_2 nanorods-graphene (TONRs-GN) composite was higher than that of TONRs alone [53]. Mohamed et al. [54] compared the photocatalytic activity for methanol oxidation of TiO_2-CNT and TiO_2-GN. Notwithstanding TiO_2-GN showed a lower band gap and higher optical absorptivity than TiO_2-CNT, the photooxidation current density of TiO_2-CNT was higher than that of TiO_2-GN, due to the strong binding between CNTs and TiO_2, the oxygen vacancies created on TiO_2 and the lower charge transfer resistance. As previously reported, the use of TiO_2 nanoparticles as photocatalysts presents some drawbacks, such as low surface area, high charge recombination rate and large electronic band gap, resulting in only UV light absorption. A promising way to improve the photocatalytic activity is the use of titanium nanotubes (TONTs). The have larger surface area, faster electron transport and lower charge recombination rate, due to the1D channel for electron transportation, than TONPs [55,56]. The structural and electronic properties of anatase TiO_2 nanotubes were investigated using density-functional theory (DFT) based calculation methods and their effect on the band gap was evaluated [57–61]. Even though TONTs have a lower bandgap than TONPs, however, they still can hardly absorb visible light. In all cases the band gap decreased with tube diameter. Band structure and density of states (DOS) show discrete energy levels at the top of the valence band and immediately below the Fermi level. This groundwork of electronic structure calculations predicts a possible band gap modification of the TiO_2 nanotube structure compared to the bulk. Significant electronic structural differences with the change in dimensions (radius) of the nanotube were observed [59]. However, whereas the results of various works [57–60] indicated that the band gap of nanotubes was lower than the band gap of TiO_2 nanoparticles, Wang et al. [61] found an opposite result. A bang gap of TONTs higher than that of bulk TiO_2 was also observed by Madura and Evarestov [62], although they used a different calculation method. Ranjitha et al. [63] produced an experimental evaluation of the TONT band gap: they synthesized TiO_2 nanotubes by an hydrothermal method, and observed band gap values of 3.6 eV and 3.5 eV for TONTs prepared using 10 h and 16 h reaction time, respectively, both lower than the band gap of bulk TiO_2. Grasser et al. [64] compared the MOR photoactivity of TONTs and TiO_2 nanoparticle (P25). The maximum catalyst activity of the TiO_2 nanotubes was *ca.* seven times that of P25. In addition to tube diameter, also the length and the aspect ratio (length/diameter ratio) affect the photocatalyic activity of TONTs. Light absorption and charge recombination, influencing the photo-activity in an opposite way, both increase with nanotube length [65], and the photocatalytic MOR activity of TONTs increases with increasing the nanotube aspect ratio, due a larger TiO_2 active surface area, important to produce photo-induced electron-hole pairs, but also to adsorb the reactants [66]. Thus, to achieve a good catalytic activity, it is highly desirable to use TONTs having a high aspect ratio and a small tube diameter. Among different method to fabricate TONTs, electrochemical anodization is the most utilized. As reported in different reviews [67–70], TONT structural characteristics, such as length, tube diameter and aspect ratio, can be tailored by modifying the anodization parameters, such as applied voltage, time and temperature. The applied voltage and anodization time strongly affect the length and diameter of TONTS: there is a general consensus that the length and tube diameter increase with increasing anodization voltage and time, the magnitude of the increase depending on anodization conditions, such as fluoride concentration, pH, water content, temperature and current density. The effect of temperature on the length and diameter of TONTs, instead, is not as clear as in the case of voltage and anodization time. Bath temperature mainly influences the morphology and the ordering the self-organized nanotubes, going from irregularly ordered pores to well ordered pores with increasing temperature [70]. There is a temperature limit (*ca.* 40 °C), however, above which the nanotubular structure was not stable. [70,71]. Conflicting results regarding the effect of temperature on TONT length were reported. Macak et al. [72] observed a linear increase of the length (*ca.* four times) with increasing temperature from 0 to 40 °C, whereas a decrease in length (*ca*, two times) with increasing temperature was found by Lim et al. [71] and Mor et al. [73]. Also the effect of temperature on tube diameter is not well determined. Some papers reported an increase in tube diameter with increasing anodization temperature [70–72]. Conversely, no change in tube diameter with electrolyte temperatures was observed in other works [73,74]. Butail et al. [75] studied the kinetics of TONT formation during electrochemical anodization of Ti films. The model suggests that TONT growth rate (r) depends on temperature and applied voltage as:

$$r = A \exp[(\gamma P - Eo)/kT] \quad (10)$$

where A, γ and K are constants and Eo is the activation energy of the process.

A model to evaluate the dependence of the length of the nanotubes on anodization conditions was proposed by Cortes et al. [76]. The dependemce of length on voltage and anodization time (and fluoride and water concentration) is shown in Eq. (11):

$$L = APtF^2W^{-1}\exp(\alpha P) + C(1 - \exp(\beta t))PW^{-1} \quad (11)$$

in which *L*, P, t, *F* and *W* are tube length, applied potential, anodization time, fluoride concentration and water concentration, respectively, and A, C are empirical constants depending on solvent properties, and α and β are empirical constants depending on temperature. Eq. (11) shows that the length is an exponential function of voltage, meaning that the process is voltage activated. The change in tube length is almost a linear function of time and highly dependent on fluoride concentration.

Regarding the aspect ratio, the formation of small diameter TONTs with enough length (high aspect ratio) is still a challenge, as both the length and diameter decrease with applied voltage and anodization time, and remarkable chemical dissolution takes place at low voltage anodization. To overcome this drawback, Wang et al. [77] proposed a two-step anodization process from high to low voltage, which allows to obtain high aspect-ratio TONTS with small diameter.

Finally, the MOR activity of TiO_2 can be improved by coupling with a metal oxide, particularly WO_3 (active under visible light illumination) [78,79]. The main absorption edge of the TiO_2/WO_3 nanocomposite shifts toward the visible region, with an improvement of the absorption intensity. Cold sprayed TiO_2/WO_3 photoelectrodes on titanium metal substrates showed higher photoelectrochemical activity for methanol oxidation than the benchmark photocatalyst TiO_2 P25 [78]. A TiO_2/WO_3 nanocomposite film presented a photocatalytic activity five times higher than that of pure TiO_2 film and eight times higher than that of pure WO_3 film [79]. The formation of a TiO_2/WO_3 heterojunction enhances the charge separation efficiency, thus increasing the lifetime of photo-generated electron–hole, which results in a higher photocatalytic activity of the TiO_2/WO_3 nanocomposite film compared to pure WO_3 and TiO_2 films.

It has to be promptly pointed out, however, that the MOR activity of

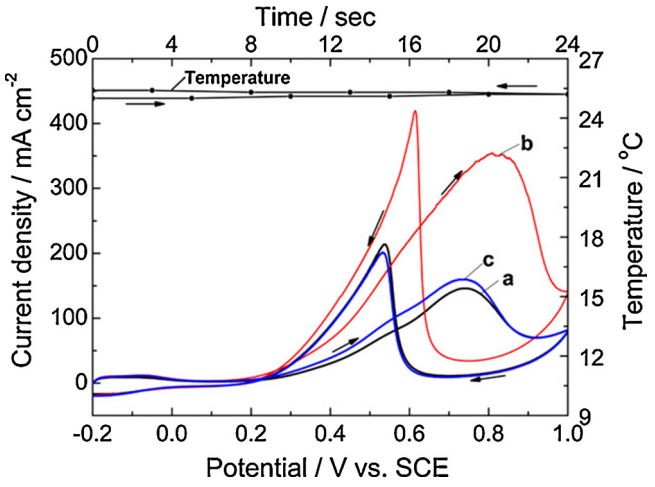

Fig. 3. Comparison of the CV under UV–vis light irradiation at 25 °C (b) with that at 25 (a) or 27 °C (c) without light irradiation. Pt–C/GC electrode, scan rate: 50 mV s − 1. The temperature was monitored during CV measurements under UV–vis light irradiation. Reproduced from Ref. [81], copyright 2012, with permission from Elsevier.

TiO_2 under illumination is considerably lower than that of Pt in dark conditions.

3.2. Photo-assisted MOR on Pt

The removal of adsorbed CO is considered a rate determining step for the MOR: by (2 + 1) resonance-enhanced multiphoton ionization and reflection absorption infrared spectroscopy it was observed that UV-light irradiation can induce CO desorption from Pt as the chemical bond between Pt and CO is changed by the excitation of a Pt electron to the 2π state *via* the Pt conduction band [80]. The threshold energy of neutral CO desorption lies between 2.3 and 3.5 eV suggesting that an unoccupied 2π state is responsible for the desorption. Li et al. [81] carried out CV measurements on a Pt/C electrode in a methanol solution in dark conditions and under UV–vis light irradiation. As can be seen in Fig. 3, the current density for methanol oxidation remarkably increased under illumination. As methanol and water do not absorb light with wavelengths between 300 and 660 nm, the reactivity of methanol or water is not enhanced during MOR upon illumination. The absence of a distinct current when a carbon-modified electrode was tested with or without light irradiation indicated no effect of carbon on the photochemical reaction. A slight temperature increase near the Pt/C electrode was observed during UV–vis light irradiation at 212 mW cm^{-2} illuminance for 4 min. However, the effect of temperature increase caused by UV–vis light irradiation on the MOR activity was negligible (Fig. 3). Moreover, the maximum value of the current density of methanol oxidation was nearly independent of the rotation rate (0, 400 and 2000 rpm), showing that methanol oxidation is poorly influenced by the mass transfer. The improvement of the MOR activity under illumination was ascribed to the enhancement of CO electrooxidation by the help of the oxygen-containing species formed on the Pt catalyst under UV-light irradiation. However, apart from Li et al. [67], only Arulmani et al. [82] observed a not negligible effect of illumination on the MOR on bare Pt. No effect was observed by Polo et al. [83] and Li et al. [84], and only a slight effect was found by Ye et al. [85]. More investigations are needed to confirm the effectiveness of illumination on the MOR activity of pure Pt.

3.3. Synthesis and photo-assisted MOR on Pt/TiO_2 and $Pt\text{-}M/TiO_2$ (M = Ru, Ni) catalysts

3.3.1. Synthesis of Pt/TiO_2 and $Pt\text{-}M/TiO_2$ photocatalysts

The preparation of Pt/TiO_2 photocatalysts is quite similar to that of Pt/TiO_2 electrocatalysts, by using the same chemical and electrochemical synthesis methods. Platinization is commonly carried out on preformed TiO_2 materials, either commercial TiO_2 powders (the most used is P25, formed by 75% anatase and 25% rutile) or homemade TiO_2 nanoparticles or nanostructured TiO_2, particularly one-dimensional structures, alone or in a composite form with carbon or metal oxide materials. The most utilized method for Pt deposition/incorporation onto/into TiO_2 supported films to prepare Pt/TiO_2 photocatalysts was the electrodeposition, using both potentiostatic and galvanostatic techniques [5,86–90]. Thin-film Pt/TiO_2 electrodes were prepared also by means of galvanic replacement of pre-deposited Cu, followed by immersion of Cu/TiO_2 into a chloroplatinic acid solution [91], and RF magnetron Pt and TiO_2 co-sputtering deposition [47]. Platinization of TiO_2 powders was carried out by chemical reduction of Pt complexes (polyol synthesis [83], microwave assisted polyol synthesis [85,92], a mixed polyol/photo-deposition method [93], and $NaBH_4$ reduction [94]) in the presence of TiO_2 particles, or by chemical (mechanical and/or ultrasonic) mixing of preformed Pt and TiO_2 nanoparticle [84,94–98]. Electrodeposition allows for an accurate control of Pt loading but requires specialized equipment, uses concentrated Pt solutions and it is difficult to apply to powder substrates. Chemical methods usually involve reducing agents and/or a high temperature annealing in a reducing atmosphere. Photodeposition is a slow process and can also lead to Pt loss. Advantages of galvanic replacement and RF magnetron sputtering are fast and room temperature processes.

3.3.2. Methanol photo-oxidation on Pt/TiO_2 and $Pt\text{-}M/TiO_2$ catalysts

The photoassisted methanol oxidation on various Pt/TiO_2 and Pt-M/TiO_2 (M = Ru, Ni) catalysts was widely investigated [5,82–106]. The effect of illumination with UV or UV–vis light on the MOR onset potential and current density of the different catalysts is reported in Table 2. All the catalysts under irradiation presented a MOR onset potential lower or even than that of the same catalysts without irradiation, indicating a positive effect of the light on methanol oxidation. An enhancement in the MOR current density was observed for all the catalysts upon illumination. As can be seen in the histogram reported in Fig. 4a, the improvement can reach up to about 200%, but the highest frequency of the MOR activity increase upon light irradiation is in the range up to 50%, then the frequency decreases with increasing the MOR current density enhancement. The averaged value of the MOR current density enhancement by irradiation was 75%. Drew et al [99] observed that MOR current on Pt-Ru/TiO_2 under UV illumination is higher than the sum of electrocatalytic current on Pt-Ru alone and photocatalytic current on TiO_2 under illumination in separate experiments at constant catalyst loadings. In the same respect, Ivanov et al. [91] observed that the current density enhancement with illumination with respect dark of Pt/TiO_2 was 344 μA cm^{-2}, much higher than the photocurrent of Pt/TiO_2 (40 μA cm^{-2}) in the methanol-free acid electrolyte and even higher than the limiting photocurrent of TiO_2 in the presence of methanol (260 μA cm^{-2}). These results indicate a synergic effect of TiO_2 and Pt or Pt-Ru catalysts in promoting methanol photo-oxidation. By splitting out the MOR activity improvement according to the TiO_2 kind, nanoparticles (TONPs, among which the most used are formed by 75% anatase and 25% rutile, namely P25) or 1 D nanostructures (TiO_2 nanotubes (TONTs), nanowires (TONWs) and nanorods (TONRs)), a shift of frequencies towards higher MOR current increase under illumination can be observed in the case of the nanostructures (see histograms in Fig. 4b). The averaged value of MOR activity improvement by illumination for 1 D TiO_2 nanostructures obtained from data in refs [86–88,90,94,98,100,102,104]. was 94%, considerably higher the mean value for TiO_2 nanoparticles of 36% from data in refs.

Table 2
Difference between the MOR onset potential of Pt/TiO_2 upon illumination (($V_o^{PtTiO2L}$) and that of Pt/TiO_2 in dark conditions ($V_o^{PtTiO2D}$), and enhancement in the MOR current density upon illumination ($(I_L-I_D)/I_D$, %). (+) $\Delta V_o(PtTiO_2L,PtTiO_2D) > 0$; (-) $\Delta V_o(PtTiO_2L,PtTiO_2D) < 0$; (=) $\Delta V_o(PtTiO_2L,PtTiO_2D) = 0$; (n.d.) not determined; I_L Current upon illumination ; I_D Current in dark conditions.

Catalyst	Medium	Light	$\Delta V_o(PtTiO_2L,PtTiO_2D)$	$(I_L - I_D)/I_D$ (%)	Reference
PtRu/ TONPs /CFE	acid	UV	–	90	[99]
Pt(Cu) TiO_2	acid	UV	–	66	[91]
Pt on tubular TiO_2	acid	UV	n.d.	20	[100]
ITO sputtered Pt/ TiO_2	acid	UV	–	30	[47]
Pt/TONTs	acid	UV-Vis	n.d.	58	[86]
Pt/TiO_2/CNTs	alkaline	UV	–	150	[92]
PtRu/TONPs mixture	acid	UV	n.d.	3-18	[83]
Pt/TONTs/Ti	acid	UV-Vis	–	150	[87]
TiO_2 photodeposited Pt	acid	UV	n.d.	9-48	[93]
Pt/TiO_2/BDD	acid	UV	=	25	[101]
Pt/TONTS	alkaline	Vis	–	31	[88]
PtNi/TONTs			–	54	
PtNi/C-TONTs	alkaline	Vis	=	14	[5]
PtNi/TONTs			=	50	
Pt/TONWs	acid	UV	n.d.	95	[94]
Pt/TONFs/C	acid	UV	=	150	[84]
Pt/TONPs	alkaline	UV-Vis	=	10	[89]
Pt/OMTiO_2	alkaline	UV	=	89	[95]
Pt/TiO_2/G-C	acid	UV-Vis	=	171	[96]
PtNFs/TONTs	acid	Vis	–	160	[102]
Pt/TONPs/GNs	acid	UV	–	66	[85]
Pt/TONPs/GNs	acid	UV	–	34	[97]
Pt TONRs	alkaline	UV-Vis	–	186	[90]
PtRu/TONPs	acid	UV-Vis	=	7	[103]
PtRu/TONPs/ CNFs				3	
Pt/TONTs	acid	UV-Vis	–	47	[98]
PtRu/TONT membrane	acid	UV	=	136	[104]
Pt/S-SMTiO_2 film	acid	UV	–	143	[105]

[83,85,89,93,97,99,103]. This result is not surprising: as reported in section 3.1, in the absence of Pt, the MOR activity of TONTs is higher than that of TONPs, due to their larger surface area, faster electron transport and lower charge recombination rate than TiO_2 nanoparticles. The higher MOR activity of Pt/TONTs than that of Pt/TONPs has to be ascribed to these best features of TONTs on TONPs. Moreover, the larger surface area of nanotubes allows a better interaction between Pt and TiO_2, improving the synergic effect under irradiation.

EIS measurements confirmed the positive effect of illumination on the MOR activity of Pt/TiO_2 catalyst [5,90,96]. In all the cases (see for example Fig. 5 from ref. [90]), the semicircle diameters on the Nyquist plots of Pt/TiO_2 under light irradiation were smaller than those in dark condition, indicating that the photo-generated electrons can improve the conductivity of the catalyst, resulting in a smaller charge-transfer resistance and thus enhancing the performance of the catalysts. In Fig. 5, the impedance plot in the second quadrant (negative Z' region) for the curves of 0 V indicates that the polarization resistance is negative. The reverse phenomenon was ascribed to the oxidation of adsorbed CO intermediate and the recovery of the catalytic sites. At more positive potentials from 0 to 0.2 V, the arcs changed to the first quadrant. This was ascribed to the platinum oxidation on the catalyst surface, resulting in the inhibition of methanol oxidation.

Fig. 6 shows the dependence of the Pt/TiO_2 MOR current density

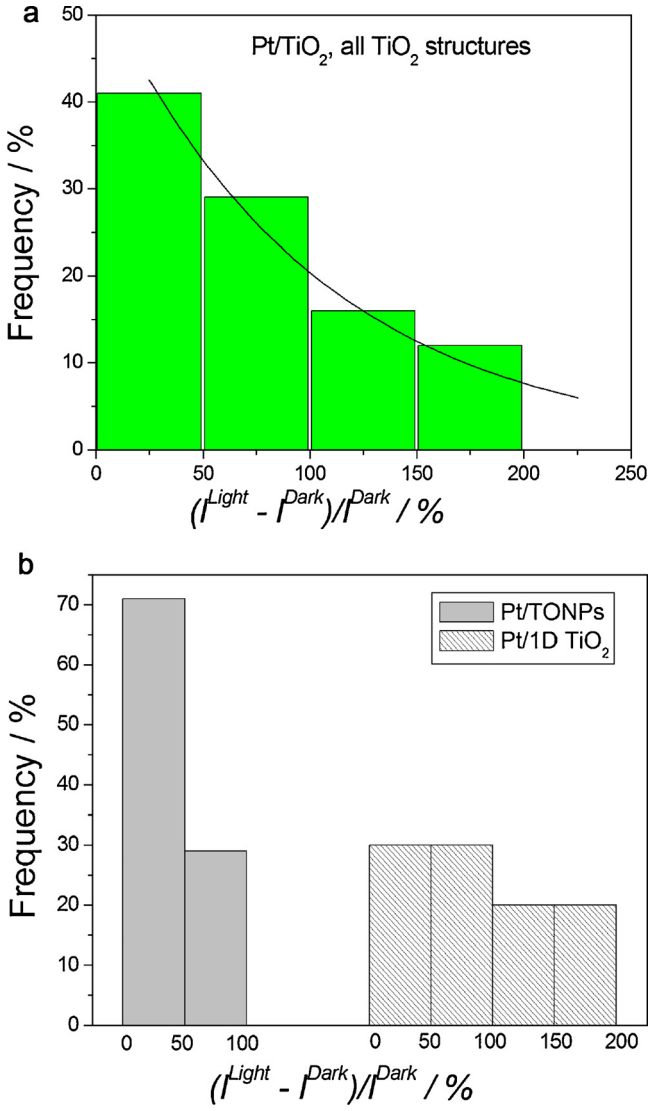

Fig. 4. Frequency of the enhancement in the MOR current density by light irradiation (A) for Pt/TiO_2 and Pt-M/TiO_2 (M = Ru, Ni; TiO_2 = all structures) and (B) for Pt/TONPs and Pt/TONTs photo-electrocatalysts.

upon illumination to Pt MOR current density in dark conditions ratio ($I_{Pt/TiO2}^{light}/I_{Pt}^{dark}$, which takes into account of both the chemical and photochemical effects of TiO_2) on the Pt/TiO_2 MOR current density to Pt MOR current density both in dark conditions ratio ($I_{Pt/TiO2}^{dark}/I_{Pt}^{dark}$, which takes only into account of the chemical effect of TiO_2) using data from different works [84,85,92,96–99]: these experimental points are interpolate by a line with a slope of 1.70 can be observed in Fig. 6. The dependence of Pt/TiO_2 MOR current density upon illumination to Pt/TiO_2 MOR current density in dark conditions ratio ($I_{PtTiO2}^{light}/I_{PtTiO2}^{dark}$, which takes into account of the light irradiation effect on Pt/TiO_2) is also reported in Fig. 6: the $I_{PtTiO2}^{light}/I_{PtTiO2}^{dark}$ ratio is almost independent of the $j_{Pt/TiO2}^{dark}/j_{Pt}^{dark}$ ratio, with the experimental points interpolated by a line with a slight negative slope of 0.08. The $I_{Pt/TiO2}^{light}/I_{Pt}^{dark}$ ratio can be expressed as:

$$I_{Pt/TiO2}^{light}/I_{Pt}^{dark} = I_{PtTiO2}^{light}/I_{PtTiO2}^{dark} * I_{Pt/TiO2}^{dark}/I_{Pt}^{dark} \quad (12)$$

On the basis of the results in Fig. 6, considering $j_{PtTiO2}^{light}/j_{PtTiO2}^{dark}$ almost constant, with an averaged value of 2, it results:

$$I_{Pt/TiO2}^{light}/I_{Pt}^{dark} = I_{Pt/TiO2}^{dark}/I_{Pt}^{dark} * 2 \quad (13)$$

that is, there is a photo-multiplicative effect of the chemical effect of

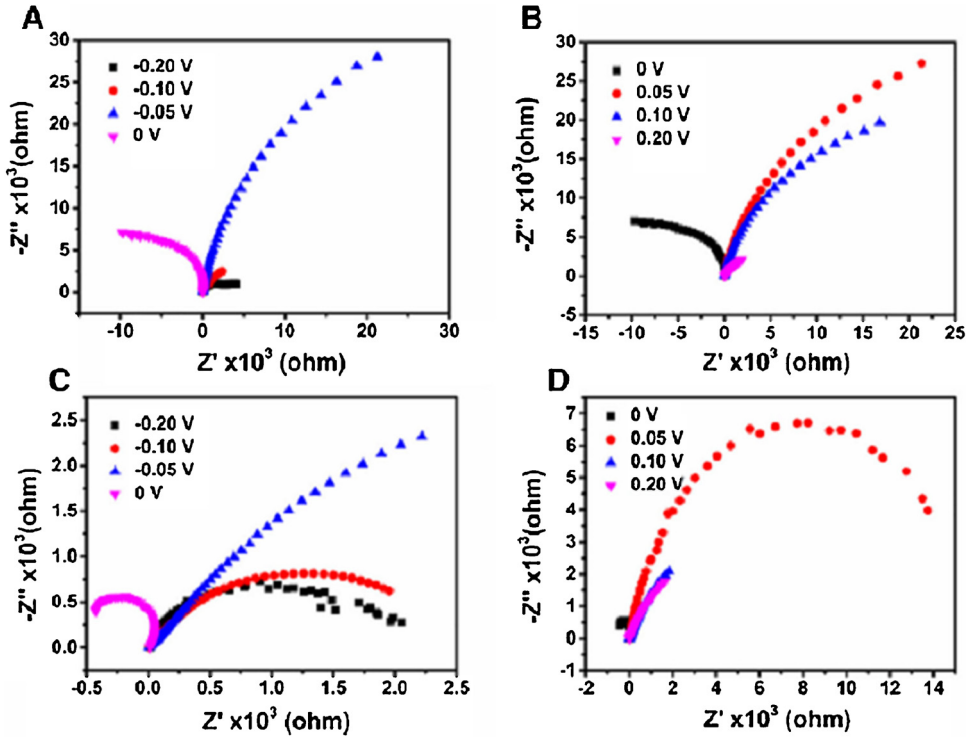

Fig. 5. EIS of Pt-1D TiO_2 nanorods without (A and B) and with (C and D) simulated solar light irradiation under different potentials. Reproduced from Ref. [90], copyright 2007, with permission from Elsevier.

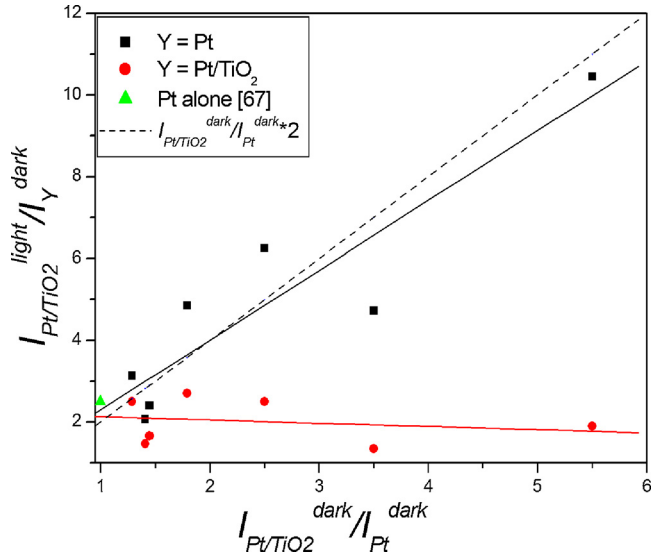

Fig. 6. Dependence of the $I_{Pt/TiO2}^{light}/I_{Pt}^{dark}$ and $I_{PtTiO2}^{light}/I_{PtTiO2}^{dark}$ ratios on the $I_{Pt/TiO2}^{dark}/I_{Pt}^{dark}$ ratio using data from different works [84,85,92,96–99]. Dashed line: $I_{Pt/TiO2}^{dark}/I_{Pt}^{dark} * 2$ *vs.* $I_{Pt/TiO2}^{dark}/I_{Pt}^{dark}$ plot.

TiO_2. As can be seen in Fig. 6, the dash line, representing the $I_{Pt/TiO2}^{dark}/I_{Pt}^{dark} * 2$ *vs.* $I_{Pt/TiO2}^{dark}/I_{Pt}^{dark}$ plot, well intersects the experimental $I_{Pt/TiO2}^{light}/I_{Pt}^{dark}/I_{Pt/TiO2}^{dark}/I_{Pt}^{dark}$ points.

Following the adsorption on platinum, the complete oxidation of methanol to carbon dioxide involves various dehydrogenation steps, followed by the oxidation of one or more intermediate species, that is, formaldehyde, formic acid and/or carbon monoxide. The process starts with the dehydrogenation of the OH group, followed by sequential dehydrogenation, and finally by oxidation of the intermediate products with the hydroxyl groups adsorbed on TiO_2 to form CO_2. A poisoning of surface active sites can occur, considering that at the start of the reaction all sites are available for methanol absorption, but additional methanol adsorption depends on the liberation of the actives sites by adsorbed intermediate species formed during the reaction initial times, which cause active site poisoning. There are two ways to evaluate the CO tolerance, that is, by cyclic voltammetry (CV) measurements through the ratio between the peak current in the forward (I_f) and the backward scan (I_b) ratio (I_f/I_b), and by chronoamperometry (CA) measurements through the amount of current retention at the steady state, expressed as $R = I_{ss}/I_0$, where I_0 and I_{ss} represent the current density at the beginning and at the steady state of CA measurements. The I_f/I_b ratio is usually used to evaluate the tolerance of the catalyst against poisoning by adsorbed species coming from the dissociative methanol adsorption, a higher I_f/I_b ratio indicating higher tolerance. On the other hand, CA is an useful tool to evaluate the poisoning of the catalyst at constant voltage. The steady-*state* current (I_{ss}) represents the equilibrium between methanol adsorption and adsorbed intermediate species oxidation: as higher is the I_{ss}, as higher is the number of active sites available for methanol adsorption and subsequent dehydrogenation and oxidation. An useful parameter to evaluate the poisoning tolerance is the percentage of current retention at the steady state ($R = I_{ss}/I_0$). An analysis of literature data, obtained by CV and CA measurements, leads to conflicting results regarding the illumination effect on the poisoning tolerance. The number of works, reporting an I_f/I_b ratio upon illumination $(I_f/I_b)_L$ lower than that in dark conditions $(I_f/I_b)_D$ [85,87–89,92,95,102], was higher than that reporting an $(I_f/I_b)_L$ ratio higher than or equal to $(I_f/I_b)_D$ [90,96,98,99]. A $(I_f/I_b)_L$ ratio lower than $(I_f/I_b)_D$ was also observed for photo-assisted methanol oxidation on Pt with mixed TiO_2-WO_3 photocatalysts [89] or with other photocatalysts, such as ZnO [107], Bi_2WO_6 [108] and CQDs-Bi_2WO_6 [108]. As it can be seen in the pie chart in Fig. 7a, the $(I_f/I_b)_L/(I_f/I_b)_D$ ratio was < 1 for 67% of the data. Conversely, for all the evaluated catalysts [47,85,87,88,90,98], with only one exception [100], it was found that the current retention upon light irradiation (R_L) was higher than the current retention in dark condition (R_D). For 88% of the data, the R_L/R_D ratio was > 1, with $R_L/R_D > 2$ for 63% of the data for 63% of the data (see the pie chart in Fig. 7b). This is surprising, as, generally, at a high

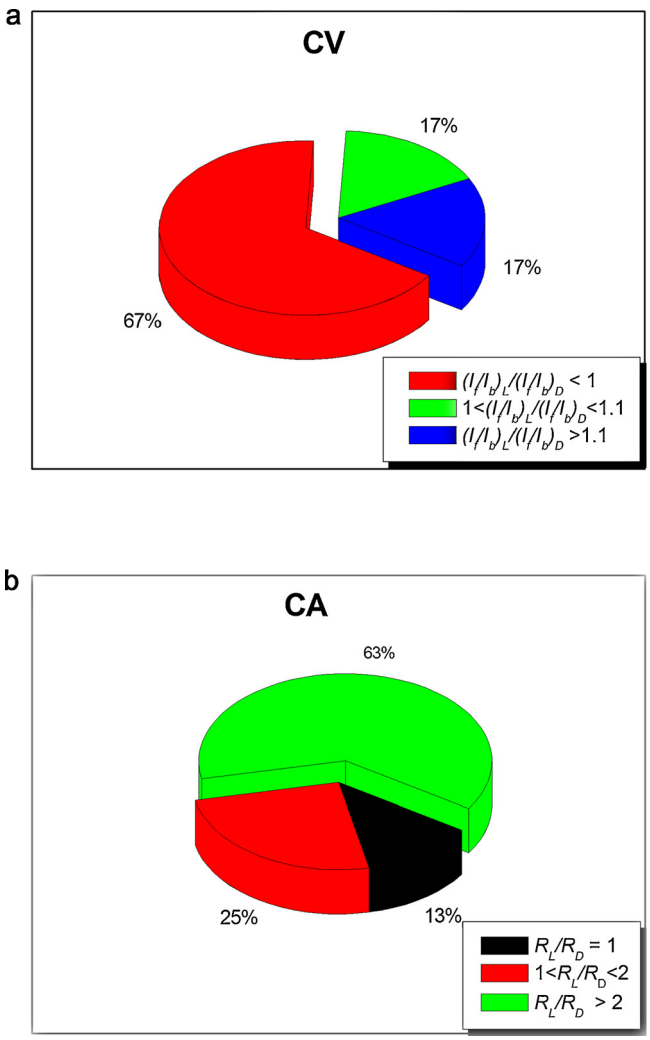

Fig. 7. Pie chart of the $(I_f/I_b)_L/(I_f/I_b)_D$ [85,87–90,92,95,96,98,99,102] (Fig. 7a) and R_L/R_D [47,85,87,88,90,98,100] (Fig. 7b) ratios.

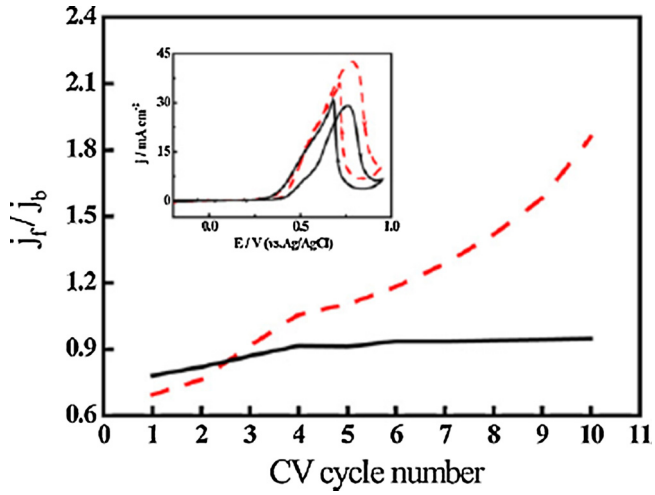

Fig. 8. The ratio of forward anode peak current density (j_f) to backward anode peak current density (j_b) of Pt/TNTs/Ti with (– – –) and without (—) illumination *vs.* cyclic voltammogram (CV) cycle number. The insert is the 6th CV cycle for Pt/TNTs/Ti in 1 M CH_3OH + 0.5 M H_2SO_4. Reproduced from Ref. [87], copyright 2011, with permission from Elsevier.

I_f/I_b by CV corresponds a high current retention by *ca.* Potential cycling confirms CA results about the positive effect of illumination on poisoning tolerance. The dependence of the I_f/I_b ratio for a Pt/TONTs catalyst with and without illumination is shown in Fig. 8 [87]. Initially the $(I_f/I_b)_L/(I_f/I_b)_D$ ratio was < 1, but starting from the third cycle the $(I_f/I_b)_L/(I_f/I_b)_D$ ratio was > 1. Indeed, in dark conditions, the I_f/I_b ratio slightly increases up to the fourth cycle, then it is almost independent of CV cycle number. Upon illumination, instead, the I_f/I_b ratio increases with cycle number, indicating that progressively Pt active sites are released with increasing cycle number. To explaining these conflicting results, we consider the basic reactions of the complete methanol oxidation to CO_2 on Pt-TiO_2 upon illumination and in dark conditions. Upon light irradiation it has:

$$TiO2 + h\nu \rightarrow TiO2 + h+ + e- \quad (4)$$

$$TiO2 + H2O \rightarrow TiO2–(H2O)ads \quad (14)$$

$$TiO2–(H2O)ads + h+ \rightarrow TiO2–(OH\cdot)ads + H+ \quad (15)$$

$$Pt + CH3OH \rightarrow Pt–(CH3OH)ads \quad (16)$$

$$Pt-(CH3OH)ads \rightarrow Pt-(CH3O-)ads + H+ \quad (17)$$

$$Pt-(CH3O-)ads + h+ \rightarrow Pt-(CH3O\cdot) \quad (18)$$

$$Pt-(CH_3O\cdot) \rightarrow Pt-(H_2CO)_{ads} + H^+ + e^- \quad (19)$$

Then H_2CO can de-adsorb or be further oxidized to CO with or without the participation of h^+:

$$Pt-(H_2CO)_{ads} + nh^+ \rightarrow Pt-CO_{ads} + 2\,H^+ + (2-n)\,e^- \ (n = 0,1,2) \quad (20)$$

Joining reaction 17–20 it obtains:

$$Pt-(CH_3OH)_{ads} + nh^+ \rightarrow Pt-CO_{ads} + 4\,H^+ + (4-n)\,e^- \ (n = (1,2,3) \quad (21)$$

Finally, CO_2 is oxidized to CO_2 by OH radicals:

$$Pt-CO_{ads} + TiO_2–(OH\cdot)_{ads} \rightarrow Pt-COOH + TiO_2 \rightarrow Pt + TiO_2 + CO_2 + H^+ + e^- \quad (22)$$

The overall reaction is:

$$CH_3OH + (n+1)\,h^+ + H_2O \rightarrow CO_2 + 6\,H^+ + (5-n)\,e^- \ (n = 1,2,3) \quad (23)$$

In dark conditions it has:

$$TiO_2 + H_2O \rightarrow TiO_2–(H_2O)ads \quad (14)$$

$$TiO_2–(H_2O)ads \rightarrow TiO_2–(OH\cdot)ads + H^+ + e^- \quad (15')$$

$$Pt + CH_3OH \rightarrow Pt–(CH_3OH)ads \quad (16)$$

$$Pt-(CH_3OH)ads \rightarrow Pt-(CO)ads + 4\,H^+ + 4\,e- \quad (21')$$

$$Pt-COads + TiO_2–(OH\cdot)_{ads} \rightarrow Pt-COOH \rightarrow Pt + TiO_2 + CO_2 + H^+ + e^- \quad (22)$$

The overall reaction is:

$$CH_3OH + H_2O \rightarrow CO_2 + 6\,H^+ + 6\,e^- \quad (23')$$

From these reactions, the following points have to be highlighted: i) the oxidation of methanol to carbon monoxide with the support of holes (reaction 21) is faster than the same reaction in dark conditions (reaction 21'), so the current density in the forward scan upon illumination (I_f) is higher than that in dark conditions (I_f'), also if the number of electrons produced by the reaction 21 is lower than those formed by the reaction 21'; ii) methoxy is a better hole scavenger than water, thus the reaction (18) is faster than reaction (15), and, as a consequence, initially photo-chemically formed OH radicals are hard to form, so the liberation of the actives sites by CO adsorbed species formed during the

first period of time, which are responsible for poisoning of the catalytic sites, takes place by chemically formed OH radicals, as in the case of dark conditions. As the number of electrons produced per unit CO formed upon illumination (4 – n, n = 1,2,3) is lower than the number of electrons produced per unit CO in dark conditions (4), it results $(I_f/I_b)_D > (I_f/I_b)_L$; iii) when the active sites are blocked by adsorbed CO, a new adsorption of methanol molecules is hindered, so the holes can react with water, that is, the reaction 10 (photo-chemical formation of OH radicals) can appreciably takes place, resulting in a faster oxidation of CO and in a higher current retention upon illumination than in dark conditions ($R_L > R_D$).

3.3.3. Photo-assisted MOR on carbon supported Pt/TiO_2 catalysts

The presence of carbon materials as the third component in Pt/TiO_2 catalysts is also important because, in addition to act as a catalyst support with high surface area and electrical conductivity, they reduce the electron/hole recombination. As previously reported, TiO_2-NCs (NCs = nanocarbons such as CNTs and GNs) composites are a suitable tool for enhancing the separation of photo-generated electron/hole pairs, due to the high electric conductivity of carbon nanomaterials. In the presence of NCs, photogenerated electrons can move towards the NC surface, which may have a lower Fermi level. In this way the NCs act as an electron sink, and the excess of holes in TiO_2 valence band can migrate to the surface and react. However, a large amount of NCs has a negative effect on the photo-oxidation, reducing TiO_2 light absorption. Different works reported the use of carbon materials as supports for Pt/TiO_2, but the comparison of the methanol oxidation in dark conditions and under illumination of Pt/TiO_2 in the presence and in the absence of carbon was reported only in one paper [103]. Ahmad et al. [103] observed that the MOR activity of Pt-Ru/TiO_2 in the presence of carbon nanofibers (CNFs) was higher than that of Pt-Ru/TiO_2 alone both in the dark and under illumination. The improvement of the MOR activity of Pt-Ru/TiO_2 in the presence of CNFs is due to the increase of the electrical conductivity of TiO_2 by CNFs addition, but, unexpectedly, the enhancement in the MOR current density upon illumination for the catalysts in the presence of CNFs was lower than that of Pt-Ru/TiO_2 alone. The titanium oxide/carbon ratio is important for a suitable MOR photo-catalysis: an optimized value of this ratio should balance the positive effect of carbon on the reduction of electron/hole recombination and its negative effect on the reduction of TiO_2 light absorption. Thus, in the Pt/TiO_2/CNFs catalyst, likely due to a high titanium oxide/carbon ratio, the negative effect of CNFs presence on TiO_2 light absorption was prevalent.

3.4. Photo-assisted MOR on Pt/MOx (M = Zn, W, and Sn)

Photo-assisted methanol oxidation was carried out also on binary catalysts formed by addition of other semiconductor photocatalyst metal oxides than TiO_2, such as ZnO, WO_3 and SnO_2, to Pt. Among them, the Pt/ZnO photocatalysts were the most investigated [107,109–111]. ZnO possess a slightly higher energy band (3.37 eV) and a higher electron mobility (115–155 $cm^2\ V^{-1}\ s^{-1}$) than TiO_2. Moreover, ZnO has similar or superior photocatalytic activity to that of TiO_2, but is less stable. The band gap of ZnO in Pt/ZnO/GNs narrowed down (2.86 eV) due to the direct attachment and intimately coupling among Pt, ZnO and GNs, allowing the absorption of visible light. As can be seen in Table 3, platinized ZnO nanoparticles [107,109] and ZnO nanorods [110,111] showed upon illumination an enhancement in the MOR current density than that of the same catalysts in dark condition, indicating a positive effect of the light on methanol oxidation. The MOR improvement under irradiation can be explained by a synergic effect between the electro-catalytic and photo-catalytic properties of Pt/ZnO catalysts, similar to that observed for Pt/TiO2 catalysts. When ZnO is irradiated by light, electrons can jump from valence band to conduction band, leaving hole in the valence band. The photo-excited electrons can improve the conductivity, whereas the holes remaining on ZnO surface will be consumed in methanol oxidation, promoting the formation of methoxy radicals and the oxidation of intermediate species to CO.

Table 3
Enhancement in the MOR current density of Pt-MO_x catalysts upon illumination $((I_L\text{-}I_D)/I_D$, %). I_L Current upon illumination; I_D Current in dark conditions.

Catalyst	Medium	Light	$(I_L - I_D)/I_D$ (%)	Reference
Pt/ZnO /C	alkaline	UV-Vis	123	[107]
Pt/ZnO/GNs	acid	UV	80	[109]
		Vis	102	
Pt/ZnO nanorods	acid	UV	62	[110]
Pt/SnO_2/GNs	acid	UV	80	[112]
		Vis	30	
Pt/WO_3/GNs	alkaline	UV	20	[113]

SnO_2 is an n-type semiconductor with a high electron mobility (~100–200 $cm^2\ V^{-1}s^{-1}$) and a band gap of 3.6 eV. Under illumination the Pt/SnO_2/GNs catalysts presents an improvement in the MOR current density than that in dark condition [112]: as can be seen in Table 3, unlike Pt/ZnO/GNs, the activity enhancement was higher under UV than under visible light, due to its wider band gap. Upon SnO_2 irradiation, the electrons jump from valence band to conduction band, and electron-hole pairs are generated. Then, the photo-catalytic mechanism for methanol oxidation was the same than that observed for Pt/TiO_2 and Pt/ZnO.

WO_3 is a semiconductor with a bandgap varying from about 2.6 to 3.0 eV, which is active under Vis light. Pt/WO_3 showed a 20% higher steady-state MOR current under visible light than in the dark [113] (Table 3). The increased catalytic activity was ascribed to both a synergic effect of Pt and WO_3 for methanol electro-oxidation at Pt sites and methanol photo-oxidation at WO_3 sites.

4. Test of Pt-TiO_2 in PDMFCs

In all the previously reported works, the electrochemical measurements were carried out in a half-cell, using a three-electrode electrochemical cell. Only a work reported a test of a Pt-Ru/TiO_2 photocatalyst in an air-breathing PDMFC [99]. Another work by the same research group reported the assembly and operation of a PDMFC, but it was used in a reverse mode for solar hydrogen production [114]. The membrane electrode assembly (MEA) was prepared by applying two carbon fiber electrodes (CFEs, 5 cm^2 each) modified with TiO_2 (0.4 mg cm^{-2}) and Pt-Ru (0.15 mg cm^{-2}) as the anode and Pt black (0.15 mg cm^{-2}) as the cathode onto the Nafion membrane. Then, the *MEA* was inserted into the air breathing PDMFC. The side facing the anode was modified with a quartz window to transmit UV light. The collector electrode was porous to allow about 40% of the electrode area to UV excitation. The photograph of the air breathing PDMFC cell under illumination and the fuel cell performance under dark and UV irradiation are shown in Fig. 9. A better performance of the PDMFC under irradiation than in dark conditions can be observed in Fig. 9. The maximum power density (MPD) values were 0.7 and 0.9 mW cm^{-2} in the absence and presence of light, respectively, that is, an improvement of 29% under illumination. These MPD values for an air-breathing DMFC are lower than those reported in literature, in the range 4–11 mW cm^{-2} [96–99], due to the dependence of fuel cell power density on the platinum loading. In the cell object of the study of Drew et al. [99], the total Pt loading (0.25 mg cm^{-2}) was 10–35 times lower than those commonly employed in air-breathing DMFCs (3–7 mg cm^{-2}) [115–118]. Another important parameter to evaluate the feasibility of fuel cells is the catalyst cost (CC), which has to be as low as possible, maintaining a suitable cell performance. In this case, the CC value for the fuel cell in dark conditions (0.35 $mg_{Pt}\ mW^{-1}$) was equal to the lower limit of the CC value literature range (0.35–1.2 $mg_{Pt}\ mW^{-1}$) and for that under illumination it was very low (0.28 $mg_{Pt}\ mW^{-1}$).

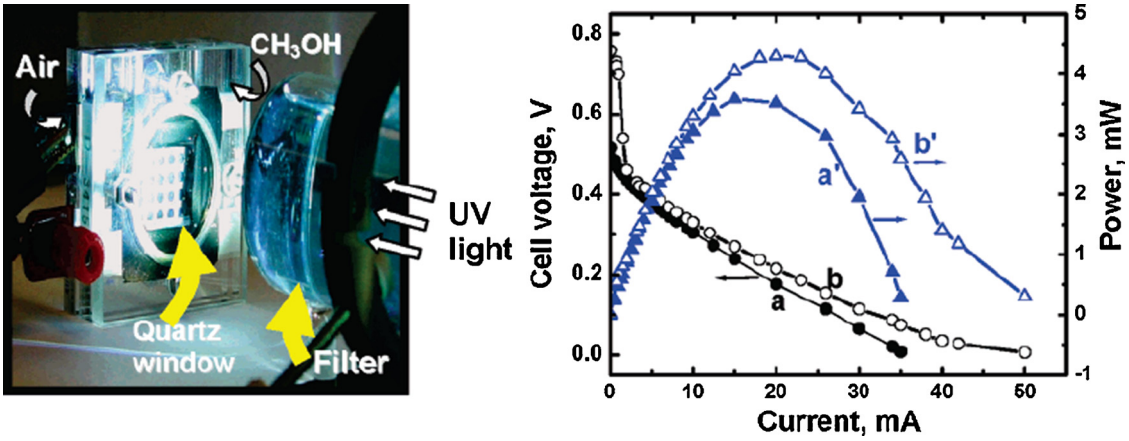

Fig. 9. Left. Air breathing DMFC cell equipped with quartz window for UV excitation. Right: Galvanostatic polarization and power output data at 295 K using Pt-Ru/TiO_2/CFE anode and Pt/CFE cathode Traces were recorded (a) and (a') in the absence and (b) and (b') in the presence of UV illumination. The Pt loadings for both cathode and anode were maintained at 0.15 mg cm^{-2} and TiO_2 loading of 0.4 mg cm^{-2}. The electrolyte was aqueous 1 M CH_3OH (electrode surface area 5 cm^2). Reproduced from Ref. [99], copyright 2005, with permission from The American Chemical Society.

5. Conclusions

A positive effect of TiO_2 addition on the activity for methanol oxidation of Pt in dark conditions has been observed. A further increases in the MOR activity of Pt/TiO_2 catalysts is obtained in the presence of light. The MOR current at Pt-TiO_2 under illumination is higher than the just sum of the current at Pt/TiO_2 in dark conditions and the photocurrent at bare TiO_2 electrodes, indicating a synergic effect of TiO_2 and Pt catalysts in promoting methanol photo-oxidation. By comparing the MOR activity of Pt/TiO_2 in dark conditions and under illumination, it results a multiplier effect of the light on the electro-catalytic activity for methanol oxidation of Pt/TiO_2 catalysts. TiO_2 nanotubes, due to their higher surface area and lower band gap, are more effective than conventional TiO_2 nanoparticles in the enhancement of the MOR activity of Pt both in dark and light condition.

The presence of carbon materials is also important for both their physical characteristics (high surface area and electrical conductivity, that make them suitable catalyst supports) and their photo-catalytic properties (charge carriers separation).

There is still plenty of room to investigate the possibilities of further increasing the beneficial effect of light on the activity and stability of carbon supported Pt/TiO_2 photocatalysts. Indeed, almost all the works focused on the photo-catalytic activity of Pt/TiO_2 catalysts in a single composition, that is, the effect of the Pt:TiO_2 ratio on the photo-assisted methanol oxidation was not evaluated. The value of the Pt:TiO_2 ratio is important as, on the one hand, its value positively affects the MOR photo-oxidation, as the light absorbance of TiO_2 in visible region increases with increasing Pt content, but, on the other hand the presence of Pt leads to a decrease of the available adsorption sites on TiO_2 surface. Thus, the optimization of the Pt:TiO_2 ratio could lead to a considerable increase in MOR activity under illumination. In the same way, the titanium oxide/carbon ratio is important for a suitable MOR photocatalysis: an optimized value of this ratio should balance the positive effect of carbon on the reduction of electron/hole recombination and its negative effect on the reduction of TiO_2 light absorption. In addition, studies on the effect of the physical characteristics of TiO_2, such as particle size and crystallinity, on the MOR photo-oxidation activity of Pt/TiO_2 photo-catalysts should also be carried out.

Considering that the MOR activity of TiO_2 can be improved by coupling with another photocatalyst metal oxide, and based on few promising works regarding Pt/TiO_2/WO_3 [89,95] and Pt/TiO_2/SiO_2 [119], the methanol photo-oxidation on Pt/TiO_2-MO_x mixed oxides (MO_x is a semiconductor photo-catalyst such as WO_3, ZnO, $FeO_{1.5}$, SiO_2 and SnO_2) instead of bare TiO_2 should be more deeply investigated.

An increase of temperature of the catalyst occurs upon illumination, which can modify the performance during long-term operation, thus an evaluation of the stability of the MOR activity under light irradiation has to be made by durability tests.

Only one test of Pt/TiO_2 photo-catalysts was carried out in PDMFC [99]. Further tests in PDMFCs have to be performed to validate both the activity Pt/TiO_2 during fuel cell operation and the photo-fuel cell technology. Moreover, the hardware of the PDMFC has to be improved: indeed, in the fuel cell tested by Drew et al [99] the porous metal collector allowed only 40% of exposure to the light of the anode. A further enhancement in the PDMFC power density can be attained by employing a collector electrode that allows the irradiation of a larger area of the anode.

References

[1] S. Wasmus, A. Küver, Methanol oxidation and direct methanol fuel cells: a selective review, J. Electroanal. Chem. 461 (1999) 14–31.
[2] T. Iwasita, Electrocatalysis of methanol oxidation, Electrochim. Acta 47 (2002) 3663–3674.
[3] N.M. Markovic, H.A. Gasteiger, P.N. Ross, X. Jiang, I. Villegas, M.J. Weaver, Electro-oxidation mechanisms of methanol and formic acid on Pt-Ru alloy surfaces, Electrochim. Acta 40 (1995) 91–98.
[4] M. Zhu, C. Zhai, C. Lu, Novel photoelectrocatalytic electrodes materials for fuel cell reactions, Adv. Electrode Mater. (2016) 435–456.
[5] H. He, P. Xiao, M. Zhou, F. Liu, S. Yu, L. Qiao, Y. Zhan, PtNi alloy nanoparticles supported on carbon-doped TiO_2 nanotube arrays for photo-assisted methanol oxidation, Electrochim. Acta 88 (2013) 782–789.
[6] E. Antolini, E.R. Gonzalez, Ceramic materials as supports for low-temperature fuel cell catalysts, Solid State Ionics 180 (2009) 746–763.
[7] E. Antolini, Composite materials: an emerging class of fuel cell catalyst supports, Appl. Catal. B: Environ. 100 (2010) 413–426.
[8] H. Lv, S. Mu, Nano-ceramic support materials for low temperature fuel cell catalysts, Nanoscale 6 (2014) 5063–5074.
[9] C. Chaiburia, V. Hacker, Catalytic activity of various platinum loading in acid electrolyte at 303 K, Energy Procedia 138 (2017) 229–234.
[10] J. Wang, G. Yin, Y. Shao, S. Zhang, Z. Wang, Y. Gao, Effect of carbon black support corrosion on the durability of Pt/C catalyst, J. Power Sources 171 (2007) 331–337.
[11] U. Diebold, The surface science of titanium dioxide, Surf. Sci. Rep. 48 (2003) 53–229.
[12] Y. Fovet, J.-L. Gal, F. Toumelin-Chemla, Influence of pH and fluoride concentration on titanium passivating layer: stability of titanium dioxide, Talanta 53 (2001) 1053–1063.
[13] N. Su, X. Hu, J. Zhang, H. Huang, J. Cheng, J. Yu, C. Ge, Plasma-induced synthesis of Pt nanoparticles supported on TiO_2 nanotubes for enhanced methanol electrooxidation, Appl. Surf. Sci. 399 (2017) 403–410.
[14] B. Hasa, E. Kalamaras, E.I. Papaioannou, J. Vakros, L. Sygellou, A. Katsaounis, Effect of TiO_2 loading on Pt-Ru catalysts during alcohol electrooxidation, Electrochim. Acta 179 (2015) 578–587.
[15] L. Zhao, Z.-B. Wang, J. Liu, J.-J. Zhang, X.-L. Sui, L.-M. Zhang, D.-M. Gu, Facile one-pot synthesis of Pt/graphene-TiO_2 hybrid catalyst with enhanced methanol electrooxidation performance, J. Power Sources 279 (2015) 210–217.
[16] B. Abida, L. Chirchi, S. Baranton, T.W. Napporn, H. Kochkar, J.-M. Léger,

A. Ghorbel, Preparation and characterization of Pt/TiO_2 nanotubes catalyst for methanol electro-oxidation, Appl. Catal. B: Environ. 106 (2011) 609–615.
[17] Q. Lv, M. Yin, X. Zhao, C. Li, C. Liu, W. Xing, Promotion effect of TiO_2 on catalytic activity and stability of Pt catalyst for electrooxidation of methanol, J. Power Sources 218 (2012) 93–99.
[18] X.-L. Sui, Z.-B. Wang, M. Yang, L. Huo, D.-M. Gu, G.-P. Yin, Investigation on C–TiO_2 nanotubes composite as Pt catalyst support for methanol electrooxidation, J. Power Sources 255 (2014) 43–51.
[19] Y. Qu, Y. Gao, F. Kong, S. Zhang, L. Du, G. Yin, Pt–rGO–TiO_2 nanocomposite by UV-photoreduction method as promising electrocatalyst for methanol oxidation, Int. J. Hydrogen Energy 38 (2013) 12310–12317.
[20] C.-S. Chen, F.-M. Pan, Electrocatalytic activity of Pt nanoparticles deposited on porous TiO_2 supports toward methanol oxidation, Appl. Catal. B: Environ. 91 (2009) 663–669.
[21] H. Song, X. Qiu, F. Li, Effect of heat treatment on the performance of TiO_2-Pt/CNT catalysts for methanol electro-oxidation, Electrochim. Acta 53 (2008) 3708–3713.
[22] K. Hirakawa, M. Inoue, T. Abe, Methanol oxidation on carbon-supported Pt–Ru and TiO_2 (Pt–Ru/TiO_2/C) electrocatalyst prepared using polygonal barrel-sputtering method, Electrochim. Acta 55 (2010) 5874–5880.
[23] L. Chen, H. Hua, Q. Yang, M.S. Javed, C. Hu, C. Zhang, Flower-structured titanium oxide with two phase coexistence supported Pt electrocatalyst for effective enhancement of electrocatalytic activity, Int. J. Hydrogen Energy 42 (2017) 5948–5957.
[24] Y.-H. Qin, Y. Li, R.-L. Lv, T.-L. Wang, W.-G. Wang, C.-W. Wang, Enhanced methanol oxidation activity and stability of Pt particles anchored on carbon-doped TiO_2 nanocoating support, J. Power Sources 278 (2015) 639–644.
[25] A.B. Kuriganova, I.N. Leontyev, A.S. Alexandrin, O.A. Maslova, A.I. Rakhmatullin, N.V. Smirnova, Electrochemically synthesized Pt/ TiO_2-c catalysts for direct methanol fuel cell applications, Mendeleev Comm. 27 (2017) 67–69.
[26] X. Wu, L. Lu, L. Li, J. Zhu, L. Mu, W. Li, Y. Zhu, X. Lu, Excellent performance of Pt-C/TiO_2 for methanol oxidation: contribution of mesopores and partially coated carbon, Appl. Surf. Sci. 426 (2017) 890–896.
[27] J. Georgieva, E. Valova, I. Mintsouli, S. Sotipopoulos, D. Tatchev, S. Armyanov, A. Hubin, J. Dille, A. Hoell, V. Raghuwanshi, N. Karanasios, L. Mallet, Pt(Ni) Electrocatalysts for methanol oxidation prepared by galvanic replacement on TiO_2 and TiO_2–C powder supports, J. Electroanal. Chem. 754 (2015) 65–74.
[28] Y. Ito, T. Takeuchi, T. Tsujiguchi, M.A. Abdelkareem, N. Nakagawa, Ultrahigh methanol electro-oxidation activity of PtRu nanoparticles prepared on TiO_2-embedded carbon nanofiber support, J. Power Sources 242 (2013) 280–288.
[29] H. Rostami, A.A. Rostami, A. Omrani, Poly (p-phenylendiamine/TiO_2) nanocomposite promoted Pt/C catalyst for methanol and ethanol electrooxidation in alkaline medium, Electrochim. Acta 91 (2016) 536–547.
[30] Z.I. Bedolla-Valdez, Y. Verde-Gómez, A.M. Valenzuela-Muñiz, Y. Gochi-Ponce, M.T. Oropeza-Guzmán, Gilles Berhault, G. Alonso-Núñez, Sonochemical synthesis and characterization of Pt/CNT, Pt/TiO_2, and Pt/CNT/TiO_2 electrocatalysts for methanol electro-oxidation, Electrochim. Acta 186 (2015) 76–84.
[31] L. Ye, Z. Li, L. Zhang, F. Lei, S. Lin, A green one-pot synthesis of Pt/TiO_2/Graphene composites and its electro-photo-synergistic catalytic properties for methanol oxidation, J. Colloid Interface Sci. 433 (2014) 156–162.
[32] R.M. Abdel Hameed, R.S. Amin, K.M. El-Khatib, A.E. Fetohi, Preparation and characterization of Pt–CeO2/C and Pt–TiO2/C electrocatalysts with improved electrocatalytic activity for methanol oxidation, Appl. Surf. Sci. 367 (2016) 382–390.
[33] C.-S. Chen, F.-M. Pan, Electrocatalytic activity of Pt nanoparticles deposited on porous TiO_2 supports toward methanol oxidation, Appl. Catal. B: Environ. 91 (2009) 663–669.
[34] A. Vittadini, A. Selloni, F.P. Rotzinger, M. Grätzel, Structure and energetics of water adsorbed at TiO2 anatase 101 and 001 surfaces, Phys. Rev. Lett. 81 (1998) 2954.
[35] M. Hepel, I. Dela, T. hepel, J. Luo, C.J. Zhong, Novel dynamic effects in electrocatalysis of methanol oxidation on supported nanoporous TiO_2 bimetallic nanocatalysts, Electrochim. Acta 52 (2007) 5529–5547.
[36] A. Fujishima, X. Zhang, D.A. Tryk, TiO_2 photocatalysis and related surface phenomena, Surf. Sci. Rep. 63 (2008) 515–582.
[37] J. Schneider, M. Matsuoka, M. Takeuchi, J. Zhang, Y. Horiuchi, M. Anpo, D.W. Bahnemann, Understanding TiO_2 photocatalysis: mechanisms and materials, Chem. Rev. 114 (2014) 9919–9986.
[38] B.H. Nguyen, V.H. Nguyen, D.L. Vu, Photocatalytic composites based on titania nanoparticles and carbon nanomaterials, Adv. Nat. Sci.: Nanosci. Nanotechnol. 6 (2015) 033001.
[39] N.S. Kolobov, D.A. Svintsitskiy, E.A. Kozlova, D.S. Selishchev, D.V. Kozlov, UV-LED photocatalytic oxidation of carbon monoxide over TiO2 supported with noble metal nanoparticles, Chem. Eng. J. 314 (2017) 600–611.
[40] Y. Zeng, W. Wu, S. Lee, J. Gao, Photocatalytic performance of plasma sprayed Pt-modified TiO_2 coatings under visible light irradiation, Catal. Comm. 8 (2007) 906–912.
[41] R. Leary, A. Westwood, Carbonaceous nanomaterials for the enhancement of TiO_2 photocatalysis, Carbon 49 (2011) 741–772.
[42] Y. Yao, G. Li, S. Ciston, R.M. Lueptow, K.A. Gray, Photoreactive TiO_2/carbon nanotube composites: synthesis and reactivity, Environ. Sci. Technol. 42 (2008) 4952–4957.
[43] A.Y. Ahmed, T.A. Kandiel, T. Oekermann, D. Bahnenamm, Photocatalytic activities of different well-defined single crystal TiO2 surfaces: Anatase versus rutile, J. Phys. Chem. Lett. 2 (2011) 2461–2465.
[44] X. Wang, A. Kafizas, X. Li, S.J.A. Moniz, P.J.T. Reardon, J. Tang, I.P. Parkin, J. Durrant, Transient absorption spectroscopy of anatase and rutile: the impact of morphology and phase on photocatalytic activity, J. Phys. Chem. C 119 (2015) 10439–10447.
[45] S. Sfaelou, P. Lianos, Photoactivated fuel cells (PhotoFuelCells). An alternative source of renewable energy with environmental benefits, AIMS Mater. Sci. 3 (2016) 270–288.
[46] T.L. Villareal, R. Gomez, M. Neumann-Spallart, N. Alonso-Vante, P. Salvador, Semiconductor photooxidation of pollutants dissolved in water: a kinetic model for distinguishing between direct and indirect interfacial hole transfer. I. Photoelectrochemical experiments with polycrystalline anatase electrodes under current doubling and absence of recombination, J. Phys. Chem. B 108 (2004) 15172–15181.
[47] K.-W. Park, S.-B. Han, J.-Min Lee, Photo(UV)-enhanced performance of Pt–TiO_2 nanostructure electrode for methanol oxidation, Electrochem. Comm. 9 (2007) 1578–1581.
[48] M. Shen, M.A. Henderson, Photochemical hole scavenging reactions of methanol on TiO2: identification of active species and water coadsorption study, AVS 59th Annual Int. Symp. Exhibition, Ehergy Frontiers Focus Topic, EN+SS-FrM2, 2012.
[49] D.A. Panayotov, S.P. Burrows, J.R. Morris, Photooxidation mechanism of methanol on rutile TiO_2 nanoparticles, J. Phys. Chem. C 116 (2012) 6623–6635.
[50] M. Setvin, X. Shi, J. Hulva, T. Simschitz, G.S. Parkinson, M. Schmid, C. Di Valentin, A. Selloni, U. Diebold, Methanol on anatase TiO_2 (101): mechanistic insights into photocatalysis, ACS Catal. 7 (2017) 7081–7091.
[51] C. Dechakiatkrai, J. Chen, C. Lynam, S. Phanichphant, G.G. Wallace, Photocatalytic oxidation of methanol using titanium dioxide/single-walled carbon nanotube composite, J. Electrochem. Soc. 154 (2007) A407–A411.
[52] R. Sellappan, J. Sun, A. Galeckas, N. Lindvall, A. Yurgens, A. Yu, D. Kuznetsov, Chakarov, Influence of graphene synthesizing techniques on the photocatalytic performance of graphene–TiO_2 nanocomposites, Phys. Chem. Chem. Phys. 15 (2013) 15528–15537.
[53] X. Li, G. Wang, L. Jing, W. Ni, H. Yan, C. Chen, Y.M. Yan, A photoelectrochemical methanol fuel cell based on aligned TiO_2 nanorods decorated graphene photoanode, Chem. Comm. 52 (2016) 2533–2536.
[54] M.M. Mohamed, S. Eid, A.Y. El-Etre, Methanol photo-oxidation at graphene and carbon nanotubes modified TiO_2 nanosheets electrocatalysts, J. Photochem. Photobiol. A: Chem. 338 (2017) 37–48.
[55] N. Liu, X. Chen, J. Zhang, J.W. Schwank, A review on TiO_2-based nanotubes synthesized via hydrothermalmethod: formation mechanism, structure modification, and photocatalytic applications, Catal. Today 225 (2014) 34–51.
[56] Y.L. Pang, S. Lim, H.C. Ong, W.T. Chong, A critical review on the recent progress of synthesizing techniques and fabrication of TiO_2-based nanotubes photocatalysts, Appl. Catal. A: Gen. 481 (2014) 127–142.
[57] V.V. Ivanovskaya, A.N. Enyashin, A.L. Ivanovskii, Electronic structure of single-walled TiO_2 and VO_2 nanotubes, Mendeleev Comm. 13 (2003) 5–7.
[58] Z. Liu, Q. Zhang, L.-C. Qin, Reduction in the electronic band gap of titanium oxide nanotubes, Solid State Comm. 141 (2007) 168–171.
[59] F.M. Hossain, A.V. Evteev, I.V. Belova, J. Nowotny, G.E. Murch, Electronic and optical properties of anatase TiO_2 nanotubes, Comp. Mater. Sci. 48 (2010) 854–858.
[60] H.-Y. Zhang, S.-L. Dong, First principles study of single wall TiO_2 nanotubes rolled by anatase monolayers, Chin. Phys. Lett. 30 (2013) 043102.
[61] J. Wang, L. Wang, L. Ma, J. Zhao, B. Wang, G. Wang, Structures, electronic properties and hydrogen-storage capacity of single-walled TiO_2 nanotubes, Phys. E 41 (2009) 838–842.
[62] A.V. Bandura, R.A. Evarestov, From anatase (1 0 1) surface to TiO_2 nanotubes: rolling procedure and first principles LCAO calculations, Surf. Sci. 603 (2009) L117–L120.
[63] A. Ranjitha, N. Muthukumarasamy, M. Thambidurai, D. Velauthapillai, S. Agilan, R. Balasundaraprabhu, Effect of reaction time on the formation of TiO_2 nanotubes prepared by hydrothermal method, Optik 126 (2015) 2491–2494.
[64] J.A. Grasser, B.K. Stover, D.S. Muggli, Synthesis factors that impact TiO_2 nanotube activity during gas-phase photocatalytic oxidation of methanol, Chem. Eng. Comm. 200 (2013) 337–350.
[65] C. Adán, J. Marugán, E. Sánchez, C. Pablos, R. van Grieken, Understanding the effect of morphology on the photocatalytic activity of TiO_2 nanotube array electrodes, Electrochim. Acta 191 (2016) 521–529.
[66] E. Mena, M.J. Martín de Vidales, S. Mesones, Javier Marugán, Influence of anodization mode on the morphology and photocatalytic activity of TiO_2-NTs array large size electrodes anodization mode on the morphology and photocatalytic activity of TiO_2-NTs array large size electrodes, Catal. Today (2018), http://dx.doi.org/10.1016/j.cattod.2017.12.036 in press.
[67] P. Roy, S. Berger, P. Schmuki, TiO_2 nanotubes: synthesis and applications, Angew. Chem. – Int. Ed. 50 (2011) 2904–2939.
[68] A. Haring, A. Morris, M. Hu, Controlling morphological parameters of anodized titania nanotubes for optimized solar energy applications, Materials 5 (2012) 1890–1909.
[69] J.-Y. Huang, K.-Q. Zhang, Y.-K. Lai, Fabrication, modification, and emerging applications of TiO_2 nanotube arrays by electrochemical synthesis: a review, Int. J. Photoenergy (2013) article ID 761971.
[70] K. Indira, U. Kamachi Mudali, T. Nishimura, N. Rajendran, A review on TiO_2 nanotubes: influence of anodization parameters, formation mechanism, properties, corrosion behavior, and biomedical applications, J. Bio- Tribo-Corros. 1 (2015) article 28.
[71] Y.-C. Lim, Z. Zainal, W.-T. Tan, M.Z. Hussein, Anodization parameters influencing the growth of titania nanotubes and their photoelectrochemical response, Int. J. Photoenergy (2012) Article ID 638017.
[72] J.M. Macak, P. Schmuki, Anodic growth of self-organized anodic TiO_2 nanotubes

in viscous electrolytes, Electrochim. Acta 52 (2006) 1258–1264.
[73] G.K. Mor, K. Shankar, M. Paulose, O.K. Varghese, C.A. Grimes, Enhanced photocleavage of water using titania nanotube arrays, Nano Lett. 5 (2005) 191–195.
[74] S. Ozkan, A. Mazare, P. Schmuki, Critical parameters and factors in the formation of spaced TiO_2 nanotubes by self-organizing anodization, Electrochim. Acta 268 (2018) 435–447.
[75] G. Butail, P.G. Ganesan, M. Raddiar, R. Teki, N. Ravishankar, D.J. Duquette, G. Ramanath, Kinetics of titania nanotube formation by anodization of titanium films, Thin Solid Films 519 (2011) 1821–1824.
[76] F.J.Q. Cortes, P.J. Arias-Monje, J. Phillips, Hugo Zea, Empirical kinetics for the growth of titania nanotube arrays by potentiostatic anodization in ethylene glycol, Mater. Des. 96 (2016) 80–89.
[77] X. Wang, S. Zhang, L. Sun, A two-step anodization to grow high-aspect-ratio TiO_2 nanotubes, Thin Solid Films 519 (2011) 4694–4698.
[78] C. Haish, J. Schneider, M. Fleisch, H. Gutzmann, T. Klassen, D.W. Bahnemann, Cold sprayed WO_3 and TiO_2 electrodes for photoelectrochemical water and methanol oxidation in renewable energy applications, Dalton Trans. 46 (2017) 12811–12823.
[79] W.T. Zhan, H.W. Ni, R.S. Chen, Z.Y. Wang, Y.W. Li, J.H. Li, One-step hydrothermal preparation of TiO_2/WO_3 nanocomposite films on anodized stainless steel for photocatalytic degradation of organic pollutants, Thin Solid Films 548 (2013) 299–305.
[80] K. Fukutani, Photodesorption of CO and CO^+ from Pt(111): mechanism and site specificity, J. Chem. Phys. 103 (1995) 2221–2228.
[81] P. Li, Z.P. Li, B.H. Liu, Methanol electrooxidation promoted by UV–vis light irradiation, J. Power Sources 199 (2012) 146–149.
[82] D.V. Arulmani, J.I. Eastcott, S.G. Mavilla, E.B. Easton, Photo-enhanced activity of Pt and Pt-Ru catalysts towards the electro-oxidation of methanol, J. Power Sources 247 (2014) 890–895.
[83] A.S. Polo, M.C. Santos, R.F.B. de Souza, W.A. Alves, Pt–Ru–TiO_2 photoelectrocatalysts for methanol oxidation, J. Power Sources 196 (2011) 872–876.
[84] W. Li, Y. Bai, F. Li, C. Liu, K.-Y. Chan, X. Feng, X. Lu, Core–shell TiO_2/C nanofibers as supports for electrocatalytic and synergistic photoelectrocatalytic oxidation of methanol, J. Mater. Chem. 22 (2012) 4025–4031.
[85] L. Ye, Z. Li, L. Zhang, F. Lei, S. Lin, A green one-pot synthesis of Pt/TiO_2/Graphene composites and its electro-photo-synergistic catalytic properties for methanol oxidation, J. Colloid Interface Sci. 433 (2014) 156–162.
[86] Z. Li, X. Cui, Y. Lin, Electrochemically synthesized ordered TiO_2 and platinum nanocomposite electrode: preparation, characterization, and application to photoelectrocatalytic methanol oxidation, J. Nanosci. Nanotech. 9 (2009) 2297–2302.
[87] Y.Q. Wang, Z.D. Wei, B. Gao, X.Q. Qi, L. Li, Q. Zhang, M.R. Xia, The electrochemical oxidation of methanol on a Pt/TNTs/Ti electrode enhanced by illumination, J. Power Sources 196 (2011) 1132–1135.
[88] H. He, P. Xiao, M. Zhou, Y. Zhang, Y. Jia, S. Yu, Preparation of well-distributed Pt–Ni nanoparticles on/into TiO_2NTs by pulse electrodeposition for methanol photoelectro-oxidation, Catal. Comm. 16 (2011) 140–143.
[89] C. Wang, F. Jiang, R. Zhou, Y. Du, P. Yang, C. Wang, J. Xu, Enhancement of methanol electrocatalytic oxidation on platinized WO_3–TiO_2 composite electrode under visible light irradiation, Mater. Res. Bull. 48 (2013) 1099–1104.
[90] S. Hu, B. Wang, H. Ju, L. Jiang, Y. Ma, Y. Fan, Photo-assisted electrocatalytic methanol oxidation based on an efficient 1D-TiO 2 nanorods arrays support electrode, J. Taiwan Inst. Chem. Eng. 80 (2017) 533–539.
[91] S. Ivanov, I. Mintsouli, J. Georgieva, S. Armyanov, E. Valova, G. Kokkinidis, I. Poulios, S. Sotiropoulos, Platinized titanium dioxide electrodes for methanol oxidation and photo-oxidation, J. Electrochem. Sci. Eng. 2 (2012) 155–169.
[92] J. Huang, J. Zang, Y. Zhao, L. Dong, Y. Wang, One-step synthesis of nanocrystalline TiO_2-coated carbon nanotube support for Pt electrocatalyst in direct methanol fuel cell, Mater. Lett. 137 (2014) 335–338.
[93] C.-T. Lin, H.J. Huang, J.-J. Yang, M.-H. Shiao, A simple fabrication process of Pt–TiO_2 hybrid electrode for photo-assisted methanol fuel cells, Microelectron. Eng. 88 (2011) 2644–2646.
[94] T. Wang, J. Tang, S. Wu, X. Fan, J. He, Preparation of ordered mesoporous WO_3-TiO_2 films and their performance as functional Pt supports for synergistic photoelectrocatalytic methanol oxidation, J. Power Sources 248 (2014) 510–516.
[95] J.-K. Oh, Y.-W. Lee, K.-W. Park, Improved photo-catalytic activity of single-crystalline TiO_2 nanowires surrounded by Pt cube nanoparticles, J. Ind. Eng. Chem. 19 (2013) 1391–1394.
[96] C. Odetola, L.N. Trevani, E.B. Easton, Photo enhanced methanol electrooxidation: further insights into Pt and TiO_2 nanoparticle contributions, Appl. Catal. B: Environ. 210 (2017) 263–275.
[97] J. Zhang, X. Hu, F. Zhu, N. Su, H. Huang, J. Cheng, H. Yang, Simple synthesized Pt/GNs/TiO_2 with good mass activity and stability for methanol oxidation, Nanotechchnology 15 (2017) 505603.
[98] J. Zhang, N. Su, X. Hu, F. Zhu, Y. Yu, H. Yang, Facile synthesis of Pt nanoparticles supported on anatase TiO_2 nanotubes with good photoelectrocatalysis performance for methanol, RSC Adv. 7 (2017) 56194–56203.
[99] K. Drew, G. Girishkumar, K. Vinodgopal, P.V. Kamat, Boosting fuel cell performance with a semiconductor photocatalyst: TiO_2/Pt-Ru hybrid catalyst for methanol oxidation, J. Phys. Chem. B 109 (2005) 11851–11857.
[100] J.M. Macak, P.J. Barczuk, H. Tsuchiya, M.Z. Nowakowska, A. Ghicov, M. Chojak, S. Bauer, S. Virtanen, P.J. Kulesza, P. Schmuki, Self-organized nanotubular TiO_2 matrix as support for dispersed Pt/Ru nanoparticles: enhancement of the electrocatalytic oxidation of methanol, Electrochem. Comm. 7 (2005) 1417–1422.
[101] T. Spataru, M. Marcu, N. Spataru, Electrocatalytic and photocatalytic activity of Pt–TiO_2 films on boron-doped diamond substrate, Appl. Surf. Sci. 269 (2013) 171–174.
[102] C. Zhai, M. Zhu, D. Bin, H. Wang, Y. Du, C. Wang, P. Yang, Visible-light-assisted electrocatalytic oxidation of methanol using reduced graphene oxide modified Pt nanoflowers-TiO_2 nanotube arrays, ACS Appl. Mater. Interfaces 6 (2014) 17753–17761.
[103] H. Ahmad, S.K. Kamarudin, L.J. Minggu, U.A. Hasran, S. Masdar, W.R.W. Daud, Enhancing methanol oxidation with a TiO_2-modified semiconductor as a photocatalyst, Int. J. Hydrogen Energy 42 (2017) 8986–8996.
[104] J.A. Díaz-Real, G.C. Dubed-Bandomo, J. Galindo-de-la-Rosa, E. Ortiz-Ortega, J. Ledesma-García, L.G. Arriaga, Evaluation of transferable TiO_2 nanotube membranes as electrocatalystsupport for methanol photoelectrooxidation, Appl. Catal. B: Environ. 222 (2018) 18–25.
[105] S. Wu, J. He, J. Zhou, T. Wang, Y. Guo, J. Zhao, X. Ding, Fabrication of unique stripe-shaped mesoporous TiO_2 films and the performance as a novel photo-assisted catalyst support for DMFC, J. Mater. Chem. 21 (2011) 2852–2854.
[106] C.Q. Wang, F.X. Jiang, R.R. Yue, H.W. Wang, Y. Du, Enhanced photo-*electrocatalytic performance of Pt/RGO/*TiO_2 on carbon fiber towards methanol oxidation in alkaline media, J. Solid State Electrochem. 18 (2014) 515–522.
[107] X. Hu, C. Ge, N. Su, H. Huang, Y. Xu, J. Zhang, J. Shi, X. Shen, N. Saito, Solution plasma synthesis of Pt/ZnO/KB for photo-assisted electrooxidation of methanol, J. Alloys Comp. 692 (2017) 848–854.
[108] H. Zheng, P. Niu, Z. Zhao, Carbon quantum dot sensitized Pt@Bi_2WO_6/FTO electrodes for enhanced photoelectro-catalytic activity of methanol oxidation, RSC Adv. 7 (2017) 26943–26951.
[109] Z. Li, L. Ye, F. Lei, Y. Wang, S. Xu, S. Lin, Enhanced electro-photo synergistic catalysis of Pt (Pd)/ZnO/graphene composite for methanol oxidation under visible light irradiation, Electrochim. Acta 188 (2016) 450–460.
[110] C.-Y. Su, Y.-C. Hsueh, C.-C. Kei, C.-T. Lin, T.-P. Perng, Fabrication of high-activity hybrid Pt@ZnO catalyst on carbon cloth by atomic layer deposition for photo-assisted electro-oxidation of methanol, J. Phys. Chem. C 117 (2013) 11610–11618.
[111] Z. Li, Z. Liu, B. Li, D. Li, Y. Fang, Low-loading platinum decorated aligned ZnO nanorods and their photocatalytic and electrocatalytic applications, J. Mater. Sci.: Mater. Electron. 26 (2015) 3909–3915.
[112] F. Lei, Z. Li, L. Ye, Y. Wang, S. Lin, One-pot synthesis of Pt/SnO_2/GNs and its electro-photo-synergistic catalysis for methanol oxidation, Int. J. Hydrogen Energy 41 (2016) 255–264.
[113] J. Georgieva, S. Sotiropoulos, E. Valova, S. Armyanov, N. Karanasios, Methanol oxidation and photo-oxidation at Pt/WO_3 electrocatalysts on graphite substrates, J. Electroanal. Chem. 727 (2014) 135–140.
[114] B. Seger, P.V. Kamat, Fuel cell geared in reverse: photocatalytic hydrogen production using a TiO_2/Nafion/Pt membrane assembly with no applied bias, J. Phys. Chem. C 113 (2009) 18946–18952.
[115] Y. Tang, W. Yuan, M. Pan, B. Tang, Z. Li, Z. Wan, Effects of structural aspects on the performance of a passive air-breathing direct methanol fuel cell, J. Power Sources 195 (2010) 5628–5636.
[116] M. Higa, K. Hatemura, M. Sugita, S. Maesowa, M. Nishimura, N. Endo, Performance of passive direct methanol fuel cell with poly(vinyl alcohol)-based polymer electrolyte membranes, Int. J. Hydrogen Energy 37 (2012) 292–301.
[117] W. Yuan, Y. Tang, Z. Wan, M. Pan, Operational characteristics of a passive air-breathing direct methanol fuel cell under various structural conditions, Int. J. Hydrogen Energy 36 (2011) 223–249.
[118] J.J. Martin, W. Qian, H. Wang, V. Neburchilov, J. Zhang, D.P. Wilkinson, Z. Chang, Design and testing of a passive planar three-cell DMFC, J. Power Sources 164 (2007) 287–292.
[119] X.L. Fan, C.X. Zhang, H.R. Xu, H. Guo, L. Song, J.P. He, Fabrication of SiO2 incorporated ordered mesoporous TiO2 composite films as functional Pt supports for photo-electrocatalytic methanol oxidation, RSC Adv. 5 (2015) 78880–78888.